Circuits of Dynamically Interacting Sigma Factors in Single Cells

Thesis by

Jin Park

In Partial Fulfillment of the Requirements
For the Degree of
Doctor of Philosophy

California Institute of Technology
Pasadena, California

2018

(Defended Aug 9, 2017)

Acknowledgements

I am indebted to my advisor Michael Elowitz for all his guidance. I first heard of Michael when I was an undergraduate and assigned his paper *Stochastic Gene Expression in a Single Cell*. This paper sparked my interest in systems biology, and the seed of the idea that I might want to pursue this field. When I came to Caltech as a graduate student and met in Michael in person, I was struck by his zeal for pursuing new, innovative ideas and his relentless drive toward clarifying and defining elegant science. I learned from Michael that clear expression of ideas is equivalent to understanding those ideas, and I take away his many lessons on scientific pursuit and presentation. More personally, I'd like to thank Michael for his patience in guiding a naive graduate student through a complicated project. It couldn't have been easy, and over the years I've become more aware of the thought he puts into mentoring. Thank you for the opportunity, this experience has been invaluable.

I would like to thank James Locke, a former postdoc who was my immediate mentor in the lab during my first two years. James trained me in the day of day to work of *B. subtilis,* and to this day I still use the basic lessons he showed me on data analysis. His supportive messages from abroad in Cambridge were much appreciated, especially because he offered support even after he had no longer official obligation to do so.

I also want to express my thanks to the other members of the timesharing team: Maria, Sofi, Marta and Jordi. This project would not have been possible without you all, and that is not an exaggeration.

I also had the fortune of working with great summer and rotation students, Jihoon Lee, Kibeom Kim, and Suzy Beeler. It's amazing how fun and easy things can be when you work with smart and hardworking people, and I thank them for all their insights and hard effort.

And to my Committee: Richard Murray, Paul Sternberg, and Lea Goentoro, I need to my express my thanks. It may not seem like much to you all, but your support has been valuable throughout this process.

Finally, I want to thank all my friends in the Elowitz lab, past and present. You made it a joy to come to work everyday, and I learned so much from you all both personally and professionally. In my early years in the lab, one friend told me that as a postdoc, he felt an obligation to help the younger graduate students find their feet. That was great for me!, but I didn't understand the sentiment at the time. I think I now do, since when you have received from others you want to pay it forward. I already miss the late night tea times, and all the discussions ranging from the downright inane to the extremely serious. I'm grateful I've gotten to know you all and sad my time with you is coming to an end.

Abstract

How do cells integrate multiple, dynamic genetic circuits? I study this question in the context of the alternative sigma factors of *B. subtilis*.

The first project proposes a novel mode of gene regulation called timesharing. The key idea is that a limited resource is shared dynamically in time. Here we show that the alternative sigma factors of *B. subtilis* use dynamic sharing to share a limited supply of core RNA Polymerase (RNAP). We show that 5 alternative sigma factors activate in pulses, and that these pulses operate in a competitive regime. Interestingly, we found that pairwise correlations between these sigma factors contained a mixture of positive and negative correlations, whereas one may naively expect all correlations to be negative. We show with a mathematical model that competitive pulsing can lead to non-intuitive sets of mixed correlations.

The second project take a closer, quantitative look at sigma factor competition. Although competition between the housekeeping sigma and a single alternative sigma has been well studied, competition between alternative sigmas themselves has been relatively unexplored. To address this issue, we systematically investigated the pairwise competitive relationships between 7 alternative sigma factors in *B. subtilis*. The main experimental tool was a 7x7 'deletion' matrix of strains, where every matrix strain was deleted for one sigma, and reported on another sigma via a fluorescent reporter. The deletion matrix revealed that competition is highly asymmetric. Deletion of any given sigma factor increased σ^W activity, but did not affect other sigma factors. These results are recreated by a minimal mathematical model of sigma factor competition, where importantly σ^W is relatively high in abundance but weak in affinity for core RNAP. We used the model to predict how overexpressing sigma factors affect each other, and these predictions were matched by experiments.

The third project reports a novel activator for alternative sigma factors. Alternative sigmas factors are activated by many forms of stress, such as nutrient limitation, temperature shifts, and molecular stresses like antibiotics. Here we show that surprisingly, cell lysis causes adjacent cells to specifically activate σ^X. This cell lysis-σ^X response is a general phenomenon, as it is observed under multiple experimental conditions. We show this relationship between cell death and σ^X is causal, since harvested cell extract activates σ^X. Finally, we hypothesize that cell death and σ^X play an important role in biofilm wrinkle formation.

PUBLISHED CONTENT AND CONTRIBUTIONS

Park J, Dies M, Lin Y, Hormoz S, Smith-Unna SE, Quinodoz S, Hernández-Jiménez MJ, Garcia-Ojalvo J, Locke JCW, Elowitz MB. Molecular Time Sharing through Dynamic Pulsing in Single Cells. Cell Syst. 2018 Mar 28;6:1-14. doi: 10.1016/j.cels.2018.01.011

J.P participated in conception, experiments, analysis, mathematical modeling, and writing of the manuscript.

Contents

Chapter 1. Introduction

I divide this Introduction into 3 parts, each part an Introduction for Chapters 2-4 of this thesis. Chapters 2-4 are the 3 main projects I present, which are:

1) Molecular time-sharing through dynamic pulsing in single cells
2) σ^W creates asymmetry in sigma factor competition
3) Cell death activates σ^X in neighboring cells, a novel mode of sigma factor activation

1.1 Molecular time-sharing through dynamic pulsing in single cells

In the 1960's, it had been shown that mixing purified RNA Polymerase (RNAP) with double-stranded DNA and ribonucleoside triphosphates in a test tube would result in RNA synthesis[1]. These experiments were exciting because they suggested a key fact now taken for granted, that RNAP performs the first step of the central dogma, transcribing DNA into messenger RNA (and that's why the enzyme was so named). This discovery of RNAP's central function opened up another important question: how does RNAP discriminate among different target DNA sites *in vivo*?

A clue to answering this question came from Richard Burgess and Andrew Travers in 1969, when they showed that a subunit of RNAP in *E. coli*, which they deemed *sigma factor*, was responsible for promoter recognition[2]. In their discussion they hypothesized that "switching sigma factor could provide the molecular basis for RNAP discrimination of target promoters". This hypothesis provided an elegant solution to the RNAP promoter selectivity problem, where RNAP simply needed to switch to an *alternative* sigma factor to transcribe a different set of target genes.

This hypothesis was borne out when the first alternative sigma factor was identified by Richard Losick's group in soil bacterium *Bacillus subtilis* in 1979[3,4]. They critically took advantage of *B. subtilis* cells' ability to turn into *spores*, hypothesizing that if alternative sigma factors existed, sporulation would represent an ideal space to identify them, as sporulation would likely utilize a very different set of sigma factors versus those used in exponential growth. This study resulted in the first identification an alternative sigma factor, named σ^B. The alternative sigma factor stands in contrast to the *housekeeping* sigma factor, σ^A, which is active during exponential growth (and which was first purified by Robert Tijan and Richard Losick[5])

In subsequent decades, a total of 17 alternative sigma factors have been identified in *B. subtilis*, and each sigma factor is associated with different functions. Five of these 17 sigma factors are associated with sporulation, and the remaining 12 are associated with a variety of stress conditions. These sigma factors are generally inactive when cells are grown in rich media, and turn on in response to their cognate stresses. For instance, σ^B is known as the *general* stress response factor because it activates in response to variety of stresses, including heat, pH, and osmotic stress[6]. In contrast, other sigma factors respond to a more limited set of conditions. For instance, σ^V responds to lysozyme, an antimicrobial peptide, but does not otherwise activate in response to a variety of other stresses[7,8].

How are sigma factors activated in response to stress? There have been many studies exploring how sigma factors are kept inactive when not needed. One common theme that has emerged is that of anti-sigma factors, proteins that bind 1:1 to sigma factors and effectively sequester them away from core RNAP, which work as follows. A sigma factor and its cognate anti-sigma factor are co-expressed, such that the anti-sigma factor concentration is greater than the sigma factor's. In this case, the anti-sigma is effectively sequestering sigma factor away from the anti-sigma factor. When the cell feels the requisite

stress, the anti-sigma factor releases the sigma factor such that the sigma factor is bound. There are a variety of molecular mechanisms by which the anti-sigma factor 'releases' the sigma factor. For instance, the anti-sigma factor of σ^W is proteolytically degraded[9,10]. In contrast, the anti-sigma factor for σ^D is exported from the cell.

In addition, it has become appreciated that core RNAP may exist in limited supply in *B. subtilis*. Michael Hecker's group performed single cell proteomics on B. subtilis and found that measured the concentration of RNAP was less than the total concentration of sigma factors in single cells[11]. In a functional approach to study sigma factor competition, a paper from Carol Gross's group demonstrated that overexpression of σ^A downregulated the activity of another sigma, σ^H, a result consistent with competition[12]. Outside of *B. subtilis*, many papers have demonstrated in *E. coli* that overexpression or underexpression of one sigma results in the opposite effect in another sigma, another result that suggests sigma factors compete[13–15].

RNAP is not the only core enzyme that may shared inside the cell. Other examples of shared core enzymatic machinery include protein degradation complexes and the ribosome. Here we study how cells approach the problem of a limited resource in the context of the alternative sigma factors of *B. subtilis*, which share a common pool of core RNAP.

Studies of sigma factor competition typically assume that sharing of RNAP is static[16,17]. In these studies, the proportion of core RNAP taken up by any given sigma class is relatively constant over time. However, previous work from our lab has shown that sigma factor activity can be time-dynamic[18]. That sigma factors can respond dynamically suggests that sharing of core RNAP can also be dynamic.

Here we propose a novel mode of sharing, which we call timesharing. In timesharing, a single class of sigma takes up most of the available RNAP for some set amount of time, and then switches to another class of sigma taking up most of available RNAP, and then this process repeats itself. This represents a completely different approach to sharing a limited resource, since at any given moment of time, most of the resource is devoted towards a single agent, rather than being spread across multiple agents.

The experimental stress we use to induce sigma factors is the small molecule Mycophenolic Acid (MPA), which critically activates at least 5 classes of alternative sigma factors. And in this condition we make three claims that together constitute Timesharing:

1) *Sigma factors activate in pulses.* We follow 5 sigmas' transcriptional dynamics with fluorescent reporters and single cell microscopy, and show sigmas' activities in MPA is dynamic in time. Pulsing is a key feature of the time dynamic nature of Timesharing.
2) *Sigma factors compete for core RNAP.* We present data that sigma factors compete for limited amounts of core RNAP in our conditions.
3) *Sigma factor pulses present with a mixture of negative and positive correlations.* The negative correlations between sigma pulses represent different sigma classes accessing core RNAP at different times. With regards to the positive correlations, we show with a mathematical model that counter-intuitively, positive correlations can also arise in a timesharing system.

Claims 1) and 3) above are novel results in *B. subtilis*, whereas claim 2) regarding competition has been well reported on in the microbiology literature. A more in-depth exploration of sigma factor competition is presented in Chapter 3. More broadly, we submit that this work is a novel mode of sharing in single cells, and hope that these concept inform future work even in synthetic systems, where ever increasingly

complex circuits may begin to deplete common cellular resources. Finally, we emphasize that timesharing does not contradict previously reported modes of sharing core RNAP. Cells may choose different regulation modes in different contexts.

1.2 σ^W creates asymmetry in sigma factor competition

Although the literature on sigma factor competition is extensive, it is mostly focused on competition between the housekeeping σ^{70} (of *E. coli*) and one other alternative sigma. The underlying reason is that the main question in the literature has been, how do alternative sigmas snatch away disproportionate amounts of RNAP from σ^{70} as cells transition to stationary phase? Thus there are studies on competition between σ^{70} and σ^{38}, σ^{70} and σ^{32} , and σ^{70} and σ^{54} [13,15,19,20], but few studies on competition between alternative sigmas. In addition, much of the literature is focused on small molecules or proteins that can shift the balance between σ^{70} and the alternative sigmas, such as ppGpp and DksA[21]. But although a few studies acknowledge competition between alternative sigmas can exist[15], how alternative sigmas compete against each other has largely been unexplored.

In addition, the vast majority of studies on sigma competition have been in *E. coli*, but the number of papers on competition in *B. subtilis* are quite few. In fact, I could only find 3 papers in sigma competition in B. subtilis. Two papers from Michael Hecker's group showed that in some media conditions, the total concentration of all sigmas exceeded that of core RNAP[11,12,22]. And another study from Carol Gross's group showed that overexpression of the housekeeping σ^A decreased activity of a σ^H reporter[12].

Taken together, the evidence is not completely convincing that competition exists in *B. subtilis*[1]. For instance, the measurements of RNAP and sigma concentrations are not sufficient to rule in competition.

[1] I do not have *a priori* reason why competition would exist in E. coli but not in B. subtilis. But it would not be surprising to me that different bacterial strains may choose different transcriptional strategies.

Although the numbers make competition plausible, they do not imply it outright. A complicating issue is that is unclear how many of the measured sigmas are functionally active. For instance, many sigmas have cognate anti-sigmas, which would lower the number of sigmas actively attempting to bind RNAP. One might then imagine considering the quantity $N_{RNAP} - \Sigma(N_{\sigma} - N_{anti-\sigma})$, i.e. comparing the number of core RNAP molecules to the total number of sigmas minus the total number of antisigmas. However, the situation is even further complicated by the presence of anti-anti-sigmas[23], many of whom are only putative[24]. Do to these issues, any measurements of molecule numbers are ideally accompanied by functional experiments *in vivo*, where one shows that perturbation of sigma, by under or overexpression, has the opposite effect on another sigma.

An example of such a functional experiment is the result that σ^A overexpression decreases activity of a σ^H reporter[12]. But although this result is consistent with competition, it does not completely rule out other possible mechanisms. For instance, this effect could be due to a σ^A target gene antagonizing σ^H activity. For instance, in E. coli σ^{38} drives transcription of rsd, an anti-sigma for σ^{70} [14]. To be fair, there is no known such antagonist between σ^A and σ^H. But nevertheless, there are many possible pleiotropic effects besides competition that could account for the result that σ^A overexpression decreases σ^H activity.

There are at least 3 ways around this problem of pleiotropic effects when studying competition:

1) Overexpress a sigma factor whose DNA binding site is mutated such that it can no longer bind it cognate DNA site, but whose RNAP binding site is intact.
2) Study sigma factor competition in a cell extract system, e.g. TX-TL[25]
3) Systematically study all pairwise interactions between sigma factors. Broad inhibitory relationships between sigmas is more elegantly explained by competition than encoding of multiple negative regulators.

These approaches are not mutually exclusive, and would provide multiple, supporting lines of evidence.

In this project, I take the 3rd strategy, and set out to answer whether 1) sigma factors compete in *B. subtilis*, and 2) if so, how alternative sigmas compete against each other. I consider 7 alternative sigmas of *B. subtilis* activated by a single stress condition, namely the drug Mycophenolic Acid (MPA). I study how these 7 sigmas interact *in vivo* via a 'deletion' matrix, in which I measure how the activity of any given sigma responds to the effect of deleting any other sigma. In this way, I systematically study all 42 pairwise relationships between 7 sigmas, which represents widespread, quantitative study of sigma factor competition.

The main claims are:

1) The deletion matrix reveals that deletion of any sigma increases σ^W activity.
2) A minimal mathematical model competition recreates the results of the deletion matrix.
3) Finally, as this is a work in progress, I discuss the future direction of this project.

1.3 Cell death activates σ^X in neighboring cells, a novel mode of activation for sigma factors

There are two broad categories of sigma factors, the 'housekeeping' sigma and the 'alternative' sigma factors. Each bacterial species has one type of housekeeping sigma, e.g. σ^{70} in *E. coli* or σ^A in *B. subtilis*, and this housekeeping sigma is responsible for most basal transcription inside the cell[26].

In contrast to the housekeeping sigma, a bacterial species can have many types of alternatives sigmas. For instance, there are 17 types of alternative sigma factors in B. subtilis. These sigmas are called alternative

simply because they are not the housekeeping sigma. And unlike the housekeeping sigma, these alternative sigmas typically are not active in rich media conditions, and activate in response to stress[27].

The literature has identified a wide variety stress conditions that activate alternative sigmas. A commonly studied stress condition is stationary phase of bacterial growth, during which *B. subtilis* activates the general stress response sigma σ^{B} [28]. In addition, nutrient limitation can induce sigma activity, e.g. nitrogen deprivation activates σ^{Y} . And heat shock activates σ^{B}, while cold shock activates σ^{L} [29,30]. Small molecules or proteins are another major class of activators, and examples include: lysozyme induces σ^{V} [31], cell wall antibiotics induce σ^{W} and σ^{M} [32], branched chain amino acids induce σ^{L} [33].

Here I present a novel activator of sigma factors. I report that cell lysis causes adjacent cells to activate σ^{X}, a previously unreported activator for σ^{X} and more broadly for sigma factors. This effect is independent of the cause of cell lysis, i.e. this effect exists in multiple experimental conditions. In addition, isolated cell extract activates σ^{X}, suggesting that cell lysis contains some chemical(s) or agent(s) that is a σ^{X} activator. This effect is specific to σ^{X}, as cell lysis only has minimal effects on other sigmas.

The identity of the chemicals inside cell extract that activate σ^{X} is an open question. Previous studies implicate multiple possible roles for σ^{X}. σ^{X} has been implicated in defense against cationic antimicrobial peptides, and also against H_2O_2 [34] However, these roles overlap with other sigma factors. The identity of the cell extract agent may not reflect either of these 2 possibilities and may be something else entirely.

Finally, I hypothesize and discuss how cell death and σ^{X} may play a major role in wrinkle formation of biofilms.

Chapter 2. Molecular time-sharing through dynamic pulsing in single cells

2.1 Abstract

In bacteria, alternative sigma factors regulate diverse stress responses and developmental programs. Sigma factors share a common pool of core RNA polymerase (RNAP). Sharing has been assumed to occur through partitioning of RNAP molecules among sigma factors. Using quantitative time-lapse microscopy, we analyzed sigma factor activity dynamics in individual *Bacillus subtilis* cells under energy stress conditions. We found that multiple alternative sigma factors activated in ~1 hour pulses in a stochastic and repetitive fashion. Analysis of sigma factor pairs revealed that two sigma factors rarely pulse simultaneously, and some pairs are anti-correlated. These results indicate that alternative sigma factor species effectively 'time-share,' or take turns utilizing, RNAP. Mathematical modeling revealed how time-sharing can emerge from noise-driven pulse-generating gene circuits actively competing for RNAP. Time-sharing provides a mechanism for cells to dynamically control the distribution of cell states within a population. Since core molecular components are limiting in many other biological systems, time-sharing may represent a general mode of regulation.

2.2 Introduction

Many core cellular components are shared among distinct regulatory factors or substrates in the cell. For example, the proteasome is shared by multiple substrate proteins, the ribosome by multiple mRNA species, and core RNA polymerase (RNAP) by multiple sigma factors in bacteria (Figure 2.1A,B). At steady-state, it is generally assumed that each substrate or factor utilizes an approximately constant fraction of core component molecules. In principle, however, sharing could occur *in time*. In such a

time-sharing system, the core component would effectively take turns, interacting predominantly with only one or a few of its many potential partner species at any given time (Figure 1C). Despite the familiarity of time-sharing strategies in engineered systems such as computers and communication networks, it is unknown whether, or how, time-sharing could occur in cells.

In bacteria, alternative sigma factors represent a classic example of molecular sharing. They function as subunits of the RNA polymerase holoenzyme, directing it to specific sets of target promoters [28,32,35–37] (Figure 1A). Alternative sigma factors are typically regulated through cognate anti-sigma factors, which prevent their association with core RNAP. These anti-sigma factors can be inhibited by stresses to enable sigma factor activation [38]. Recently it was shown that the alternative sigma factor σ^B in *Bacillus subtilis* is activated in a sustained series of stochastic pulses in response to energy stress [17,18]. These pulses represent events in which many σ^B molecules simultaneously become active, associate with core RNAP to initiate transcription of target genes, and then deactivate. However, σ^B is only one of 17 alternative sigma factors in *B. subtilis* [38] (Table S1). It has remained unclear whether pulsing is specific to σ^B or occurs across the broader set of alternative sigma factors, whether multiple sigma factors pulse under the same conditions, and how pulsing relates to the sharing of core RNAP.

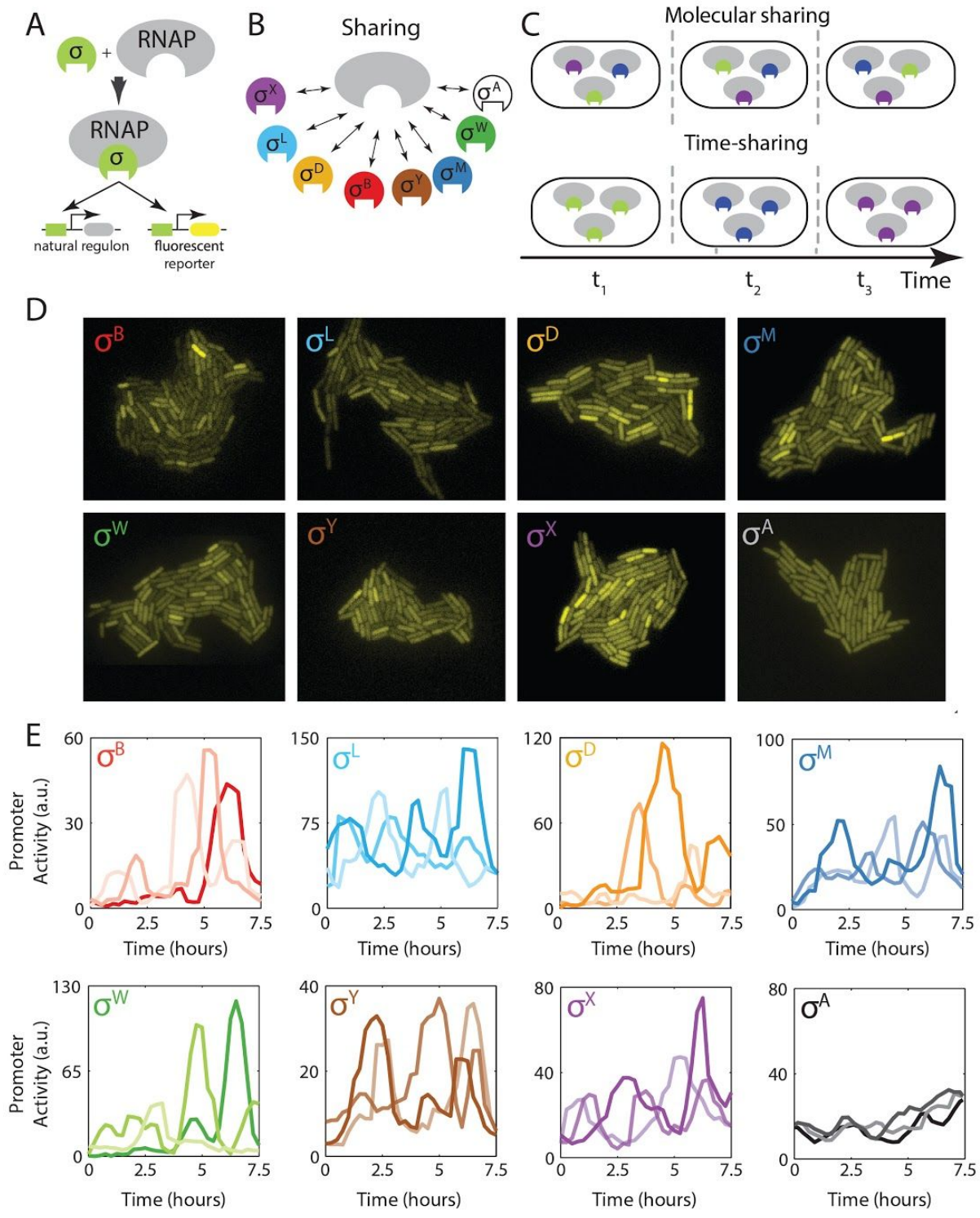

Figure 2.1. Multiple alternative sigma factors pulse under energy stress. (**A**) Alternative sigma factors bind core RNAP to activate target genes, including endogenous targets (left target) and the engineered fluorescent reporters used here (right target). (**B**) Multiple distinct alternative sigma factor species (colored shapes) share core RNAP (gray). The 'housekeeping' sigma factor σ^A (white) also utilizes core RNAP. (**C**) In principle, sigma factor

species could share core RNAP either in concentration (molecular sharing, top) or in time (time-sharing, bottom). Only 3 distinct species are shown here for simplicity. (**D**) Fluorescent reporter expression shows heterogeneous activation of seven alternative sigma factors, as indicated, and homogeneous activation of σ^A (bottom right) under energy stress conditions. (**E**) The heterogeneous expression of YFP in **D** reflects pulsing of alternative sigma factors, but not the housekeeping sigma factor σ^A, whose activity was more constant. Each plot shows sigma factor activity time traces derived from analysis of the rate of production of corresponding fluorescent reporter genes in 3 different cell lineages (different line shades).

2.3 Results

To address these issues, we constructed a set of reporter strains, each containing a fluorescent protein gene specifically activated by one of the *B. subtilis* alternative sigma factors not involved in sporulation (Figure 2.1A and 2.S1A, Table S1). We analyzed these strains in a minimal medium containing 40 μg/ml mycophenolic acid (MPA), a drug that reduces cellular ATP levels and stimulates a broad energy stress response [39] (Figure 2.S1B). Single-cell analysis of these reporter strains revealed markedly heterogeneous activation of seven alternative sigma factors in these conditions (Figure 1D). The distributions of fluorescent protein expression exhibited long tails for some sigma factors (Figure 2.S1C), similar to those previously observed under conditions of pulsatile activation of σ^B [18]. In contrast, the housekeeping sigma factor σ^A, which has higher affinity for core RNAP and lacks an anti-sigma factor [40], was activated in a more homogeneous manner, suggesting that this type of heterogeneous activation was not general to all sigma factors (Figures 2.1D and 2.S1C).

To understand the dynamic origin of this heterogeneity, we used quantitative time-lapse fluorescence imaging on growing microcolonies of our fluorescent reporter strains on agarose pads. To quantify sigma factor activity (in contrast to sigma factor abundance), we extracted total fluorescent protein levels over time in each individual cell, and computed the instantaneous rate of fluorescent protein production from its corresponding target promoter, correcting for photobleaching and dilution due to cell growth [41,42] (see

STAR Methods). This activity reflects the rate at which free sigma factor (not sequestered by its cognate anti-sigma factor) can associate with available core RNAP and initiate transcription at target promoters. It therefore depends on sigma factor protein levels, anti-sigma factor levels, and the availability of core RNAP. This analysis revealed that the seven alternative sigma factors mentioned above were activated in a pulsatile fashion (Figures 2.1E and S1D). Pulses appeared to be generated stochastically, as no significant correlations were observed in sister cell pairs (Figure S2A), or between a parent cell and its two daughters (Figure 2.S2B). Widespread stochastic pulsing of this type was not specific to MPA-induced stress, as stationary phase conditioned media also caused pulsing of many sigma factors (Figure 2.S3A), which did not require σ^B, a factor previously shown to pulse (Figure 2.S3B) [18].

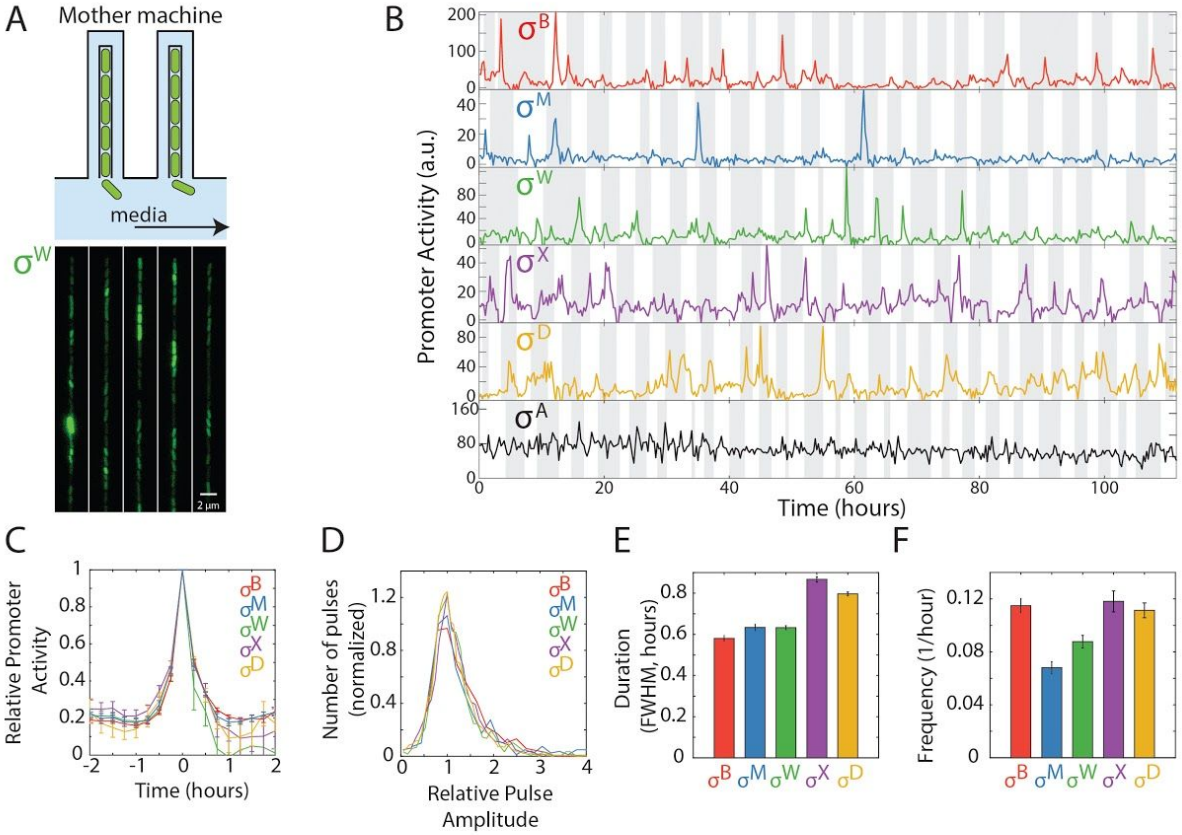

Figure 2.2. Five alternative sigma factors exhibit pulsatile dynamics over extended timescales in the mother machine. (A) The mother machine microfluidic device enables long-term analysis of a single cell lineage, as a single cell is maintained at the end of a channel (schematic, top, and image of cells in device, bottom). **(B)** Traces showing dynamics of 5 pulsatile alternative sigma factors over >100 hours. The traces represent promoter activities of target promoters for the indicated alternative sigma factors. Cell cycles are indicated by alternating gray and white vertical regions. **(C)** Mean pulse dynamics for each sigma factor species. Pulses were aligned and

averaged (n≥320). **(D)** Distribution of normalized pulse amplitudes for the indicated sigma factors. **(E)** Mean pulse durations, quantified as full-width at half maximum (FWHM) for each of the sigma factors. **(F)** Pulse frequencies for the indicated sigma factors.

We next sought to characterize the pulse dynamics more precisely. Because pulses occur much less than once per cell cycle, this required analysis over many generations. Exponential accumulation of cells on agarose pads limits the number of generations that can be analyzed, and leads to non-stationary environmental conditions. To circumvent these issues, we turned to the mother machine, a microfluidic device that enables analysis of a single cell over many cell division events [43–45] (Figure 2.2A). In the mother machine, we observed qualitatively similar dynamics as on agarose pads, with 5 alternative sigma factors exhibiting pulsatile behavior (Figure 2.2B), with strikingly similar pulse shapes (Figure 2.2C) and amplitudes (Figure 2.2D). Pulse had durations on the order of 1 hour (Figure 2.2E) and varying frequencies (Figure 2.2F). σ^Y and σ^L were not active under these conditions, and were therefore not considered further.

To understand how pulsing affects the mode of sharing of core RNAP, we constructed a mathematical model incorporating key regulatory features common to many alternative sigma factor systems (see STAR methods). These include transcriptional autoregulation, inhibition by a co-expressed anti-sigma factor, and activation by an input, here taken to be a molecular ligand that inactivates the anti-sigma factor (Figures 2.3A and 2.S4A). We identified physiologically reasonable parameters (see STAR methods) sufficient to generate pulsing dynamics similar to those observed experimentally for an individual sigma factor (Figure 2.3B). In this regime, a stochastic burst of ligand production can suddenly reduce the activity of its cognate anti-sigma factor against the corresponding sigma factor. Autoregulation of the sigma factor operon initially amplifies the pulse by up-regulating expression of the sigma factor itself. Finally, the pulse eventually terminates itself through increased expression of the anti-sigma factor, which

is part of the sigma operon (Figures 2.3B and 2.S4B). These results show that the simple sigma/anti-sigma operon architecture is capable of generating pulsatile dynamics under physiologically reasonable conditions.

We next asked how multiple pulsatile sigma factor species interact dynamically under conditions of limiting RNAP. We expanded the model to include five identical, but orthogonal, pulsatile sigma factor systems (Figure 2.3C). Additionally, to represent the constitutive, non-pulsatile σ^A (Figure 2.1E), the model also incorporated an additional sigma factor species with no anti-sigma factor. All sigma factors were coupled to one another exclusively through competition for limiting amounts of shared core RNAP (STAR methods). Such competition has been established in previous work [12,46–48], and is further supported by experiments in which ectopic expression of σ^B repressed σ^W and σ^D activity under these conditions (Figure 2.S5A, 2.S5B, 2.S5C).

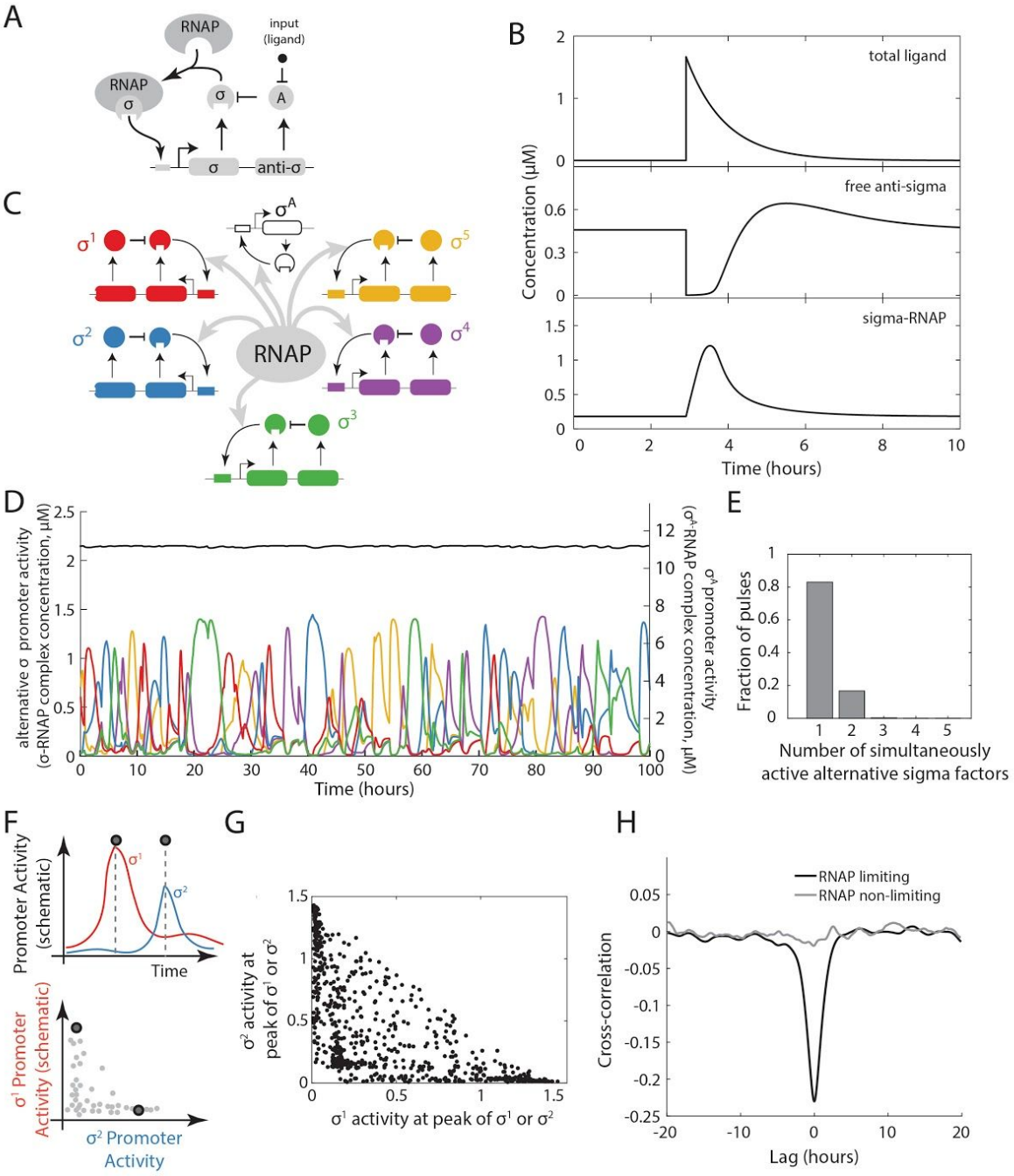

Figure 2.3. A mathematical model shows time-sharing in alternative sigma factor dynamics. (**A**) Schematic of model of a single pulsatile alternative sigma factor species. The sigma factor autoregulates its own operon, which contains genes for the sigma factor and its cognate anti-sigma factor. An input, taken to be a small molecule ligand (black dot), induces pulses by inhibiting the sigma factor inhibitory activity of the anti-sigma factor. **(B)** The simple sigma factor model can generate a pulsatile response to a sudden increase in ligand. **(C)** Multiple alternative sigma factor circuits identical to the one in (A), along with a constitutive sigma factor representing σ^A, are coupled through sharing of core RNA polymerase (gray arrows). **(D)** The multi-sigma factor model produces pulsatile dynamics of each alternative sigma factor (colored traces, left y axis) but more constant dynamics for σ^A (black, right y axis). **(E)** Histogram showing the mean fraction of sigma factors active during

pulses in the dynamics shown in (D). Most of the time, only one or two alternative sigma factors are active simultaneously. **(F)** Quantifying the co-occurrence of pulses (schematic). A pulse detection algorithm (Figure S1D) recognizes pulses in either of two sigma factors (vertical dashed lines, upper panel). Sigma factor activities at these points can then be plotted, as shown in lower panel. **(G)** Pulse amplitudes for all detected events, plotted as in the lower panel of F. Note the diagonal edge, representing the constraint of fixed total RNA polymerase. **(H)** Cross-correlation functions between the activities of two alternative sigma factors show anti-correlation between pairs of sigma factors when RNA polymerase is limiting (black) but not when it is in excess (gray).

The model generated pulsatile dynamics for each of the alternative sigma factors, and an approximately constant activity for σ^A, consistent with experiments (Figures 2.3D and 2.S5D). In this regime, nearly all core RNAP not bound to σ^A was occupied by just the 2 most active alternative sigma factors (Figure 2.3E). Furthermore, the sigma factors actively excluded one another, suppressing simultaneous pulses of multiple sigma factors (Figures 2.3F,G), and generating an overall anti-correlation in their activity when RNAP was limiting but not when it was in excess (Figure 2.3H). These anti-correlations arise because each sigma factor pulse reduces the amount of core RNAP available for other sigma factors over a typical pulse duration (~1 hour). Subsequent termination of the pulse causes the sigma factor to relinquish core RNAP, allowing other sigma factors to initiate pulses (Figure 2.S4B,2.S5D). While the overall rate of pulsing in this parameter regime is controlled by underlying stochastic inputs, represented in the model by ligand species, the exclusion of simultaneous pulsing results from competition for core RNAP. These modeling results show that time-sharing dynamics can emerge from the combination of pulsatile activation dynamics from individual sigma factor operons and coupling through competition for core RNAP.

These simulations provoke the experimental question of what dynamic relationships occur among the pulsatile sigma factors. To address this issue, we constructed a 5×5 ‘matrix’ of strains (15 strains in total, i.e. the upper half matrix plus the diagonal), each of which containing a cyan fluorescent protein (CFP) reporter for one sigma factor and a yellow fluorescent protein (YFP) reporter for a second (Figure 2.4A).

The matrix also included 'diagonal' strains containing two distinguishable reporters for the same sigma factor to establish the upper limit of possible correlation [49]. Finally, all strains contained a third fluorescent protein (mCherry) reporter for σ^A activity (see STAR Methods). Using the mother machine, we recorded movies of individual cells from each of these 15 strains (Figure 2.4B). We then quantified mean fluorescence and protein production rates for all reporter pairs over time in each individual cell lineage (Figure 2.4C).

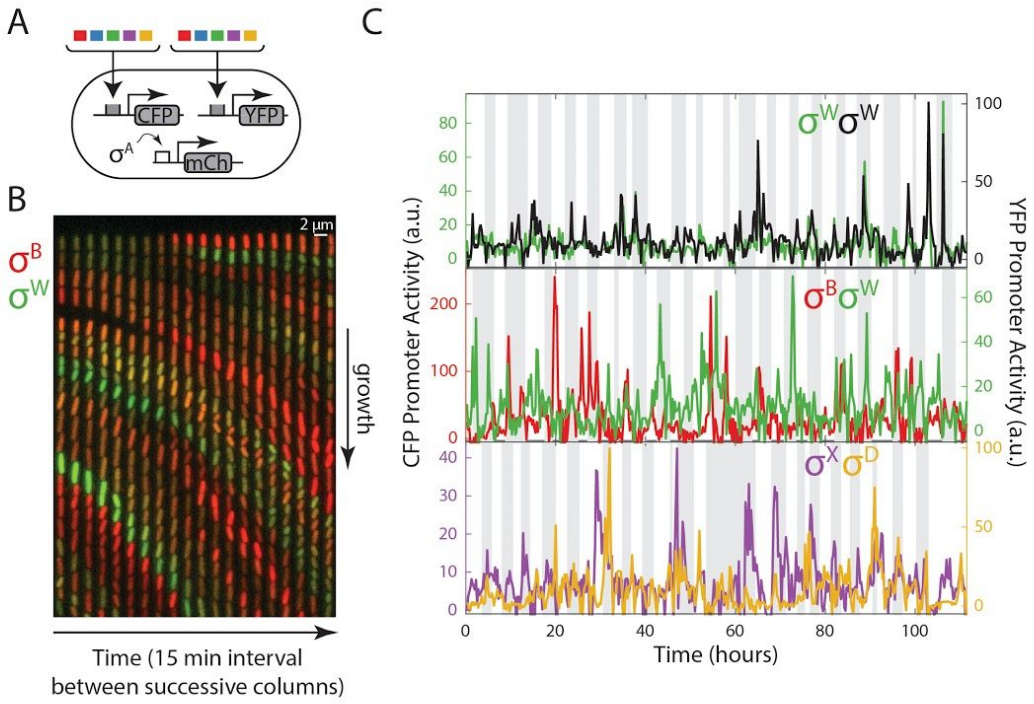

Figure 2.4. A matrix of multi-reporter strains enables analysis of dynamic correlations between different alternative sigma factors. (**A**) A matrix of strains, each of which contains a chromosomally integrated CFP reporter for one sigma factor and a chromosomally integrated YFP reporter for another, along with mCherry under the control of σ^A. (**B**) Filmstrip from a mother machine movie, showing one lane at 15 minute intervals. P_B-CFP is shown in red, overlaid with P_W-YFP in the green channel (see Movie S3). Anti-correlations between channels are apparent from the lack of cells showing similar intensities in green and red channels (i.e. yellow cells). **(C)** Typical traces showing the dynamics of different pairs of alternative sigma factors, including strains with two reporters for the same sigma factor (top), and other pairs (lower 2 panels).

Analysis of these traces provided the pairwise dynamic correlations across all five pulsatile sigma factors. As expected, strains with two reporters for the same alternative sigma factor showed strong positive

correlations (Figure 2.5A). By contrast, 4 of the 10 off-diagonal strains showed negative correlation between two different sigma factors, as predicted by the model (Figure 2.5A,B). These negative correlations were striking, given the many factors expected to positively correlate the signals, including extrinsic fluctuations in cell growth rate and global gene expression parameters (e.g. transcription and translation efficiencies) [49–53], and the co-activation of multiple sigma factors by overlapping stresses, including MPA [18,39]. The same negative correlations also appeared when using a "pulse-triggered averaging" approach that specifically focuses on pulses [54] (Figure 2.S6). Of the remaining 6 pairs, 5 showed positive correlations that were significant, although substantially weaker than those observed for diagonal strains (Figure 2.5A). Finally, one sigma factor pair showed no strong correlation in either direction. Although exhibiting different signs and degrees of correlation, the absolute frequency of pulse coincidences was low for all pairs. This can be seen by plotting together the relative strengths of the promoter activity pairs for all identified peaks (Figure 2.5C).

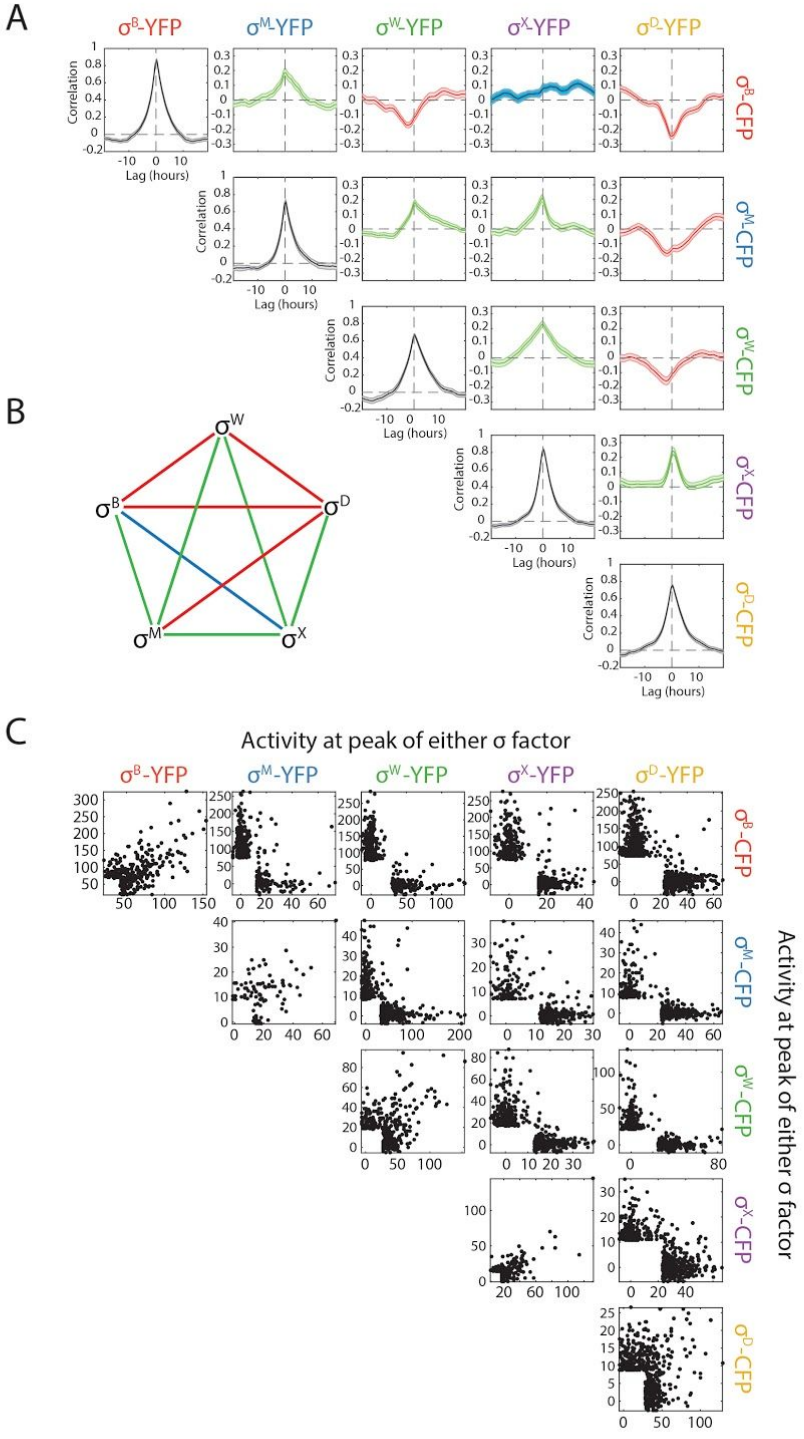

Figure 2.5. Dynamic correlations between sigma factors in the same cell. (A) The matrix of cross correlations shows both positive correlations (green), negative correlations (red), and neutral correlation (blue). Each trace shows the mean cross-correlation (solid line) and the standard error of the mean (shading). **(B)** Diagram summarizing the pattern of correlations (colors as in A). **(C)** Scatter plots of pulse event amplitudes, as in Figure 3F. Note that sigma factor pairs show relatively few simultaneous pulse events.

Together, these results provide strong evidence for time-sharing under these conditions, but they also reveal a complex dynamical structure. This can be seen in the correlation graph (Figure 2.5B), where no two sigma factors share the same pattern of correlations with other sigma factors [55]. Even σ^B and σ^D, which show similar (though not identical) interactions with the other sigma factors, are anti-correlated with one another. Could such dynamic complexity arise from competitive interactions between sigma factors? To address this question, we constructed a minimal, analytically solvable model of sigma factors competing for a common pool of core RNAP, dispensing with the regulatory features incorporated in the computational model discussed above (Figure 2.S7A). We solved this model for an arbitrary number of sigma factors under the simplifying assumption of small equilibrium fluctuations (see STAR Methods). We obtained analytical expressions for the cross-correlation functions between all sigma factor pairs in terms of the binding/unbinding rates of the sigma factors to core RNAP and their abundances. These results show that competitive binding interactions alone are sufficient to generate complex correlation graphs with mixtures of positive and negative correlations (see STAR Methods). For example, in the case of three sigma factors, it is possible for two of the sigma factors, σ^1 and σ^2, to exhibit positive correlations with each other, and negative correlations with σ^3 (Figure 2.S7B,C). This occurs when σ^3 has slower binding and unbinding rates to core RNAP compared with those of the other two. In this regime, the fraction of core RNAP bound by σ^3 fluctuates at a time scale longer than that of the other two sigma factors. At shorter time scales, σ^1 and σ^2 are both more likely to be found bound to core RNAP when the fraction of bound σ^3 is lower than its steady state value, resulting in a positive correlation between σ^1 and σ^2 (Figure 2.S7D). The analytical minimal model thus demonstrates that complex correlation patterns, including positive correlations between certain pairs of sigma factors, can arise from competitive interactions alone, even without having to invoke extrinsic correlating factors (which could also exist).

2.4 Discussion

Time-sharing causes cells to focus the limited resource of core RNAP on a few alternative sigma factor regulons at a time, rather than spreading it across all sigma factors at lower, constant levels (Figure 2.1C). Consider three hypothetical alternative sigma factors. With molecular sharing, all cells would exhibit relatively similar phenotypic states, with intermediate activities of each sigma factor, constrained by the total amount of core RNAP (Figure 2.6A, left simplex). By contrast, time-sharing causes sigma factor activities to mainly occupy the edges and vertices of the allowed state-space (Figure 2.6A, right simplex), and to dynamically transition from one such state to another in a stochastic fashion.

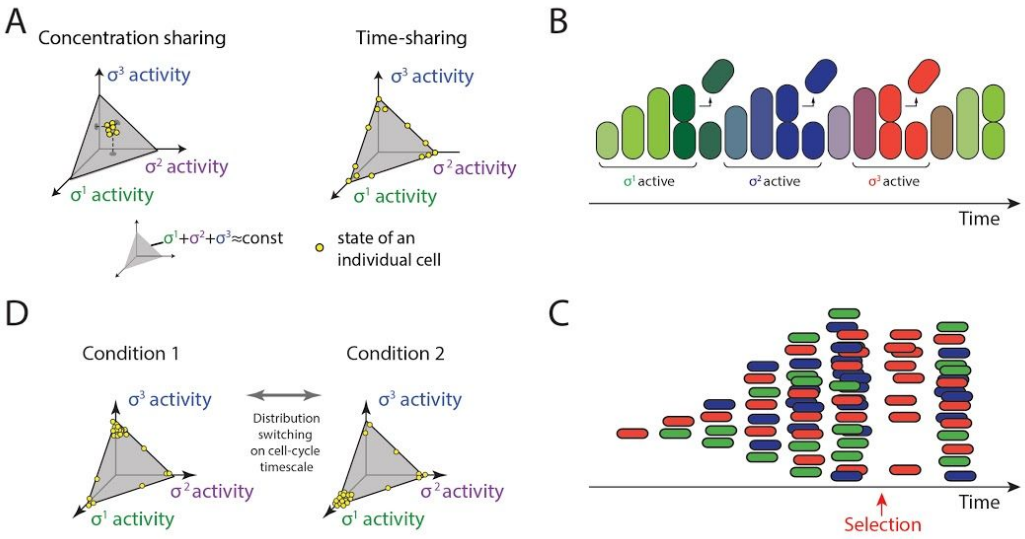

Figure 2.6. Time-sharing affects the distribution of cell states in a population. (A) Two distinct modes of sigma factor sharing (schematic). Competition for core polymerase restricts mean sigma factor activities to a subspace indicated by gray triangle, on which the sum of sigma factor activities is constant. In molecular sharing, each sigma factor would be active at a constant, intermediate level, with all cells (yellow dots) in similar states. In time-sharing, cells predominantly occupy the vertices and edges of the allowed subspace (yellow dots, right triangle), and switch dynamically among these states through pulsing. They are therefore distributed over a broader variety of expression states at any given time. **(B)** Because the timescale of pulses is comparable to the cell cycle duration, cells tend to switch states from one cell cycle to the next (schematic). Here, colors indicate activity levels of each of 3 sigmas, in a hypothetical 3-sigma factor system, following A. **(C)** A population of time-sharing cells. As in B, colors indicate activities of 3 sigma factors. Due to stochasticity of sigma factor

pulses, the distribution of cell states can recover within a cell cycle from a perturbation to the cell state distribution (red arrow). **(D)** In the time-sharing system, dynamic switching among states enables changes to the environment to rapidly shift the population from one distribution to another (left and right spaces, schematic).

Because the pulse durations observed here, of ~1 hour, are comparable to the duration of the cell cycle, time-sharing can cause successive cell cycles to be dominated by different sigma factor programs and corresponding phenotypes (Figure 2.6B). Because of the stochastic nature of pulsing, this distribution is dynamic, allowing cells to control the distribution of activity states in the population, and regenerate the entire distribution of states after a perturbation (Figure 2.6C,D). The time-sharing dynamics observed here could thus enable cells to implement a multi-dimensional bet-hedging system in which environmental conditions modulate the relative numbers of cells in which different sigma factor combinations are active [56–59]. Bet-hedging strategies can be advantageous when future events are uncertain [60] and have been shown to evolve in variable environments [61]. Pulsatile time-sharing could also provide other functional capabilities such as avoiding conflicts between incompatible regulatory programs, and increasing coordination of target operons by concentrating most target gene expression into brief periods of high sigma factor activation [62–65].

Time-sharing strategies are common solutions to the allocation of limited resources in diverse contexts. For example, time division multiplexing is used in communication systems to share limited bandwidth by switching among different users [66]. Similarly, time-sharing computer systems were developed to increase the efficiency of a core processor when the activities of individual users fluctuate [67]. Because many cellular systems rely on shared molecular components operating in competitive regimes, time-sharing may represent a dynamic design principle employed more broadly by other molecular circuits in the cell.

2.5 Supplementary Figures

Table 2.S1

Sigma Factor	Function	Group
σ^A	House Keeping	1
σ^H	Sporulation Initiation	3
σ^D	Chemotaxis	3
σ^B	General Stress Response	3
σ^E	Sporulation	3
σ^G	Sporulation	3
σ^F	Sporulation	3
σ^K	Sporulation	3
σ^I	Unknown	3
σ^M	Regulator of early stationary-phase genes	4
σ^W	Antibiotic resistance	4
σ^V	Cell wall protection	4
σ^X	Cell wall metabolism	4
YlaC	Oxidative stress response	4
σ^Y	Unknown	4
σ^Z	Unknown	4
σ^O	Unknown	4
σ^L	Amino acid catabolism	σ^{54} family

Table 2.S1. Summary of Bacillus subtilis sigma factors. For each sigma factor, we list the process or function it has been shown to be involved in, if any. We also indicate the sigma factor structural group (Paget, 2015).

Figure 2.S1

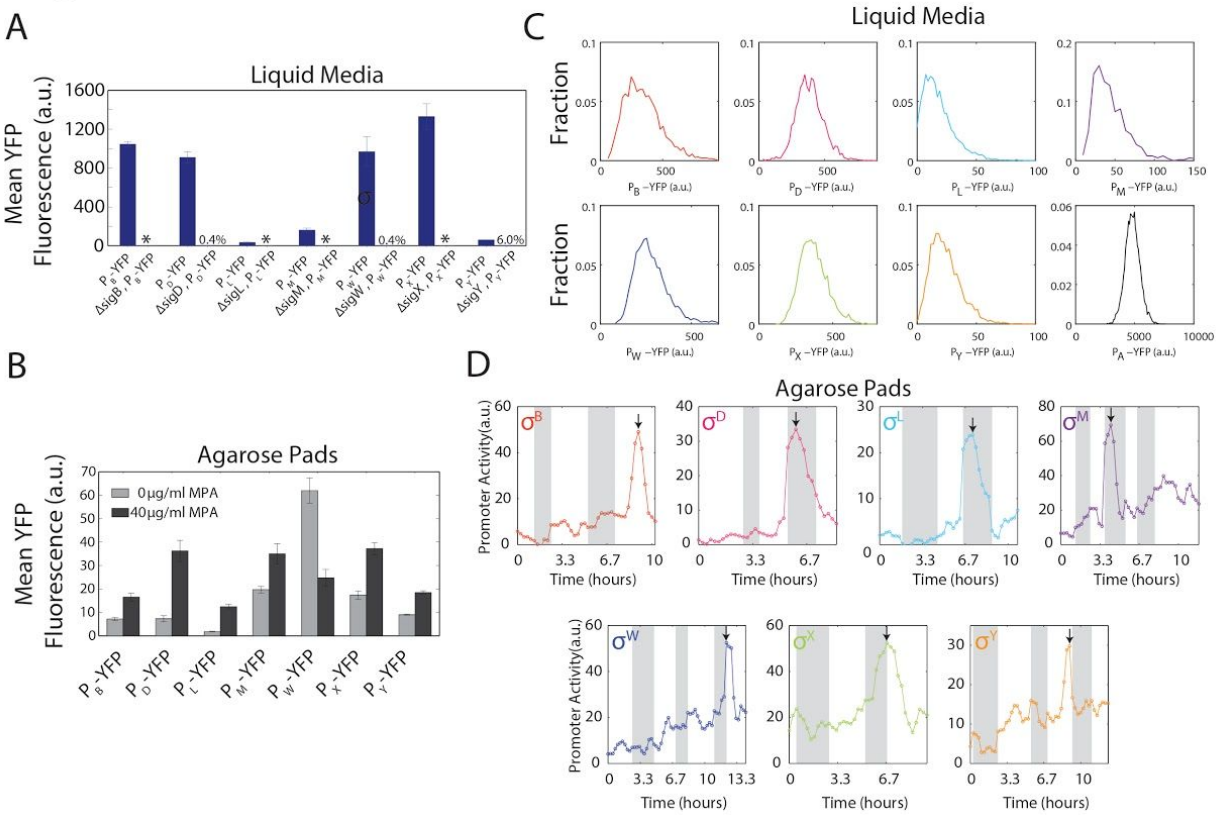

Figure 2.S1. Behavior of Sigma Factor reporters in Liquid Culture and on Agarose Pads. (A) Sigma factor reporters are specific for their cognate sigma factor. YFP reporters for each sigma factor were analyzed in the presence of 40 μg/ml MPA, either in a wild-type background or a strain in which the cognate sigma factor was deleted. Bars represent the mean fluorescence of at least 300 cells, averaged over 2 independent experiments done in liquid culture. Error bars indicate s.e.m. The percentages above bars indicate the knockout strains' mean fluorescence relative to that of the wildtype strain. * indicates fluorescence measurements indistinguishable from background.

(B) MPA activates multiple sigma factors. Sigma factor reporters were grown from single cells into small microcolonies on agarose pads of ~100 cells, with or without 40 μg/ml MPA. Each bar represents the mean fluorescence of the microcolony at its final size, averaged over at least 4 separate microcolonies from 2 independent experiments. Error bars indicate s.e.m.

(C) Sigma factors activate heterogeneously in response to MPA. For each distribution the indicated sigma factor reporter strain was grown for 3 hours in liquid culture containing 40 μg/ml MPA. Fluorescence intensities of individual cells were analyzed by quantitative microscopy. At least 3500 cells were measured per distribution.

(D) Automatic detection of promoter activity pulses. Time-lapse movies of seven alternative sigma factor reporter strains grown on agarose pads in the presence of 40 μg/ml MPA were acquired. Each time trace represents the promoter activity of a single cell lineage, with each circle representing a single timepoint. Alternating white and shaded areas indicate the cell cycle. Black arrows denote the peak of automatically identified pulses. Importantly, only local maxima passing defined thresholds are identified as pulses, to avoid misdetection of random fluctuations (see STAR Methods).

Figure 2.S2

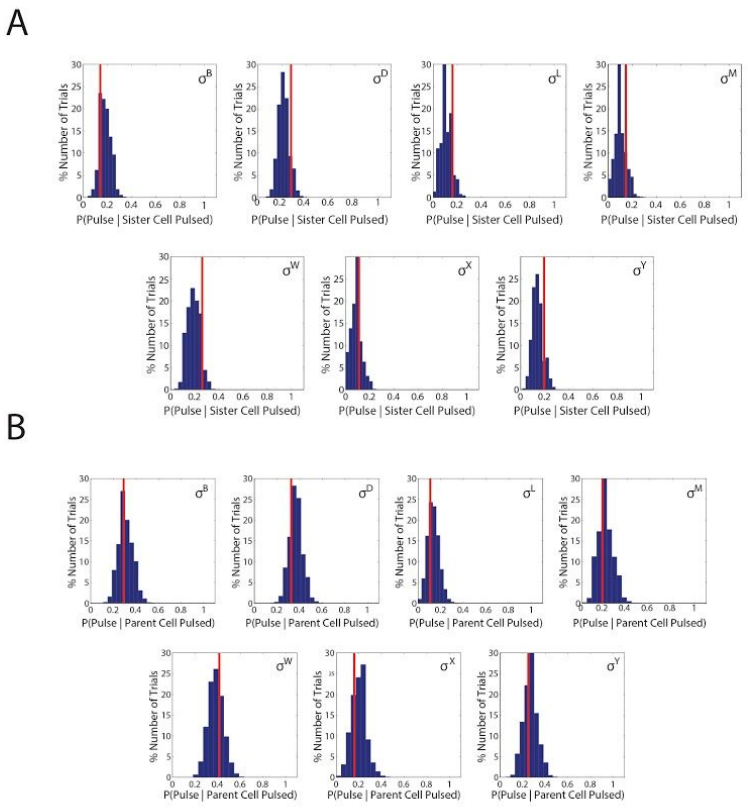

Figure 2.S2. Pulse incidence between cell relatives is not correlated. (A) Pulse incidence between cell sisters and between a parent cell and its daughter (B) is not correlated. Red lines indicate the measured frequency of two sister cells both pulsing in the same cell cycle, grown on agarose pads containing 40 μg/ml MPA. This can be compared to the distribution of expected probabilities computed from a 'null hypothesis' in which sister cell relationships are scrambled (blue histograms). Note that the measured values are well within the distribution of values expected in the absence of a correlation between sisters. Null distributions were generated with 25000 resamples.

Figure 2.S3

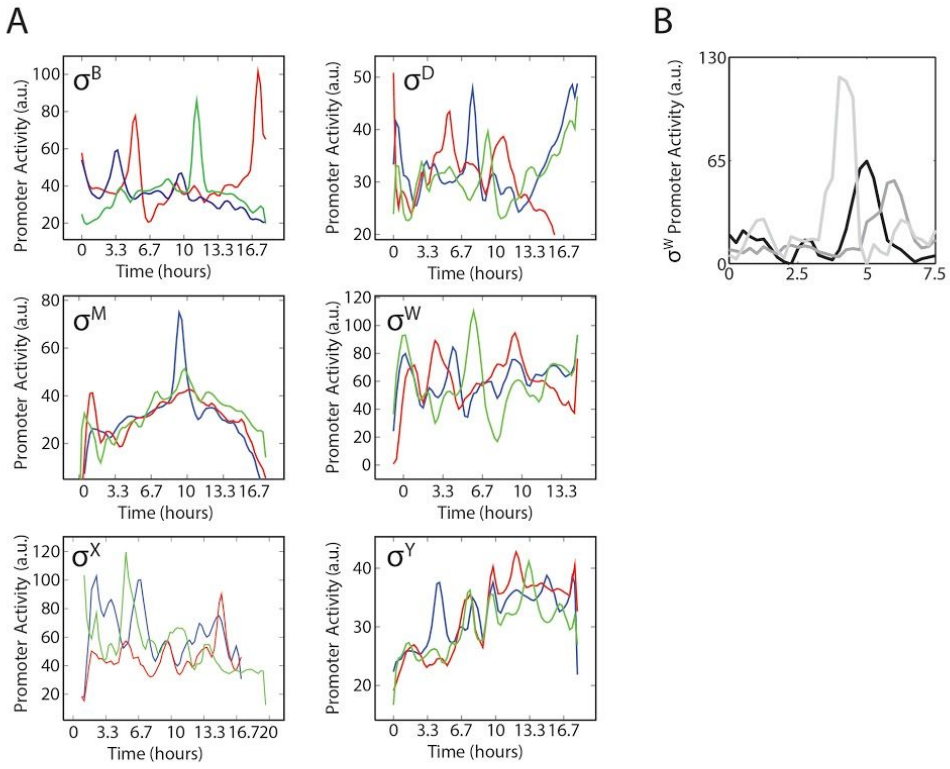

Figure 2.S3. Multiple sigma factors pulse under stationary phase conditions, and this pulsing does not require sigB. (A) Each panel shows 3 representative traces (red, green, and blue lines) of pulsing lineages of the indicated alternative sigma factor reporter strain grown on agarose pads containing conditioned media extracted from a stationary phase culture of Bacillus subtilis cells grown in LB media.

(B) Alternative sigma factor pulsing does not require sigB. 3 representative pulsing traces of a P_W-YFP reporter in a ΔsigB strain grown on agarose pads containing 40 μg/ml MPA.

Figure 2.S4

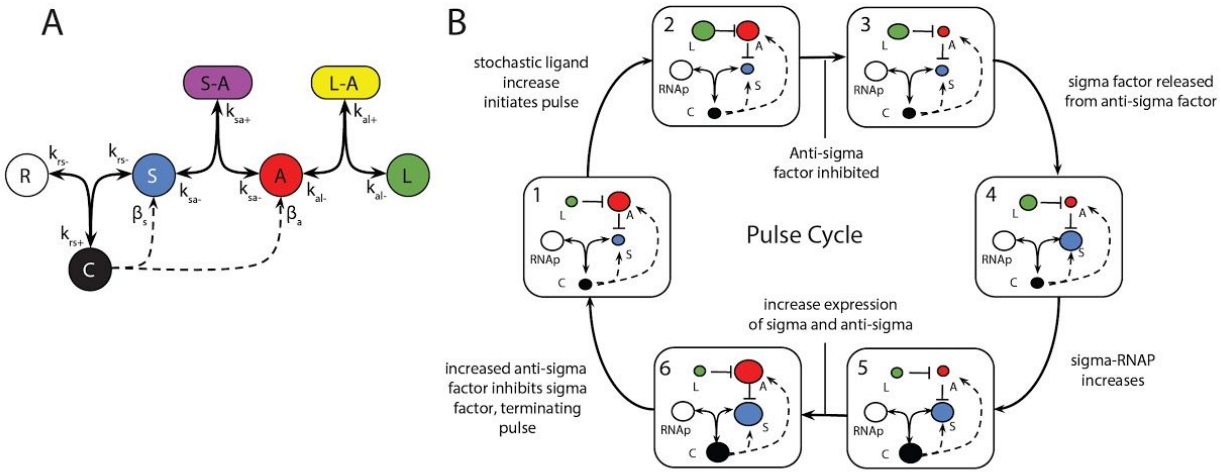

Figure 2.S4. Schematic of model reactions with pulse cycle. (A) Each alternative σ factor pathway involves a σ factor (S), a cognate anti-σ factor (A), and an input, represented as a regulatory ligand (L). Negative regulation occurs through sequestration of S by A in the S-A complex. Pulse activation is driven by competitive sequestration of A by L in the L-A complex. RNA polymerase (R) is shared between the σ factors, and the active σ factor-RNAP complex (C) upregulates the operon containing the σ factor and the anti-σ factor. Protein-protein interactions are represented by solid arrows, and transcriptional regulation by dashed arrows. Rate constants for each reaction are indicated. (B) The cycle of events that occur during a pulse are indicated by numbered boxes. In each box, the size of a component indicates, schematically, its relative abundance. Cartoons are simplified compared to A.

Figure 2.S4

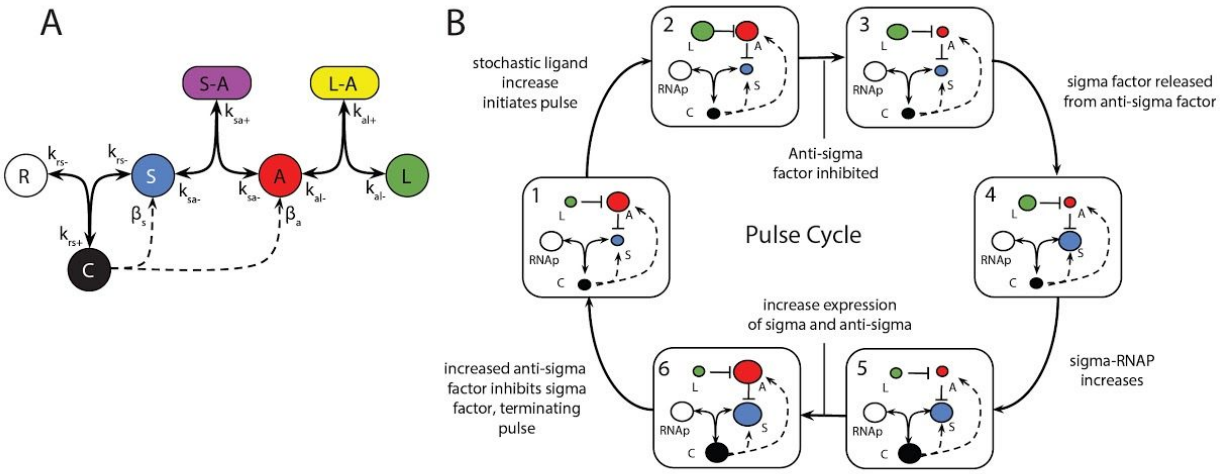

Figure 2.S4. Schematic of model reactions with pulse cycle. (A) Each alternative σ factor pathway involves a σ factor (S), a cognate anti-σ factor (A), and an input, represented as a regulatory ligand (L). Negative regulation occurs through sequestration of S by A in the S-A complex. Pulse activation is driven by competitive sequestration of A by L in the L-A complex. RNA polymerase (R) is shared between the σ factors, and the active σ factor-RNAP complex (C) upregulates the operon containing the σ factor and the anti-σ factor. Protein-protein interactions are represented by solid arrows, and transcriptional regulation by dashed arrows. Rate constants for each reaction are indicated. (B) The cycle of events that occur during a pulse are indicated by numbered boxes. In each box, the size of a component indicates, schematically, its relative abundance. Cartoons are simplified compared to A.

Figure 2.S5

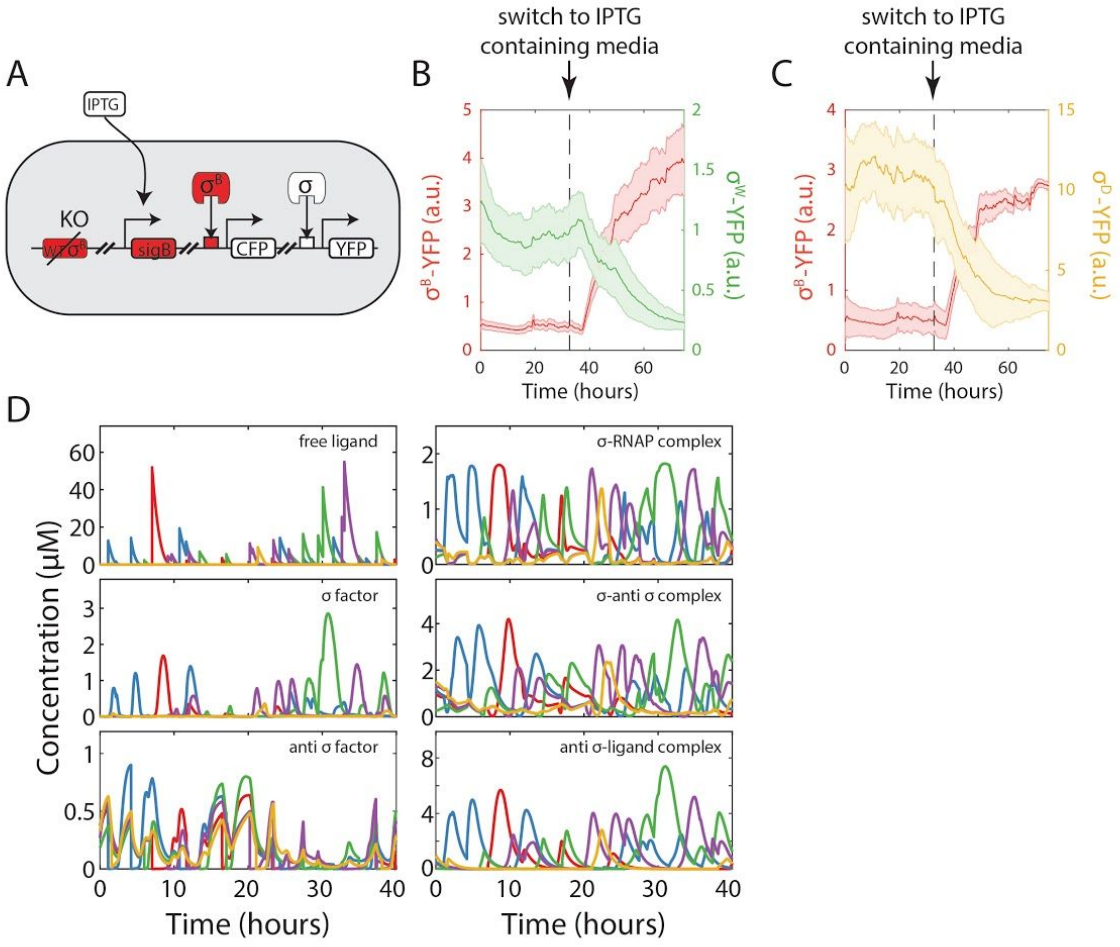

Figure 2.S5. SigB induction competes away sigW and sigD activity, and output of the 6 sigma factor model. (A) Schematic of constitutive σ^B dual reporter strain. The sigB operon was knocked out (KO) and replaced with an IPTG-inducible $P_{Phyperspank}$-sigB promoter, chromosomally integrated at the amyE locus. The strain also contained a chromosomally integrated reporter for σ^B activity, $_P$B-CFP, as well as a chromosomally integrated YFP reporter for σ^W or σ^D activity. (B,C) These strains were grown in the mother machine with minimal media containing 40 μg/ml MPA. At the indicated time, input syringes were switched to media that also contained 1 mM IPTG. Each trace represents the average of 50 (B) or 23 (C) traces, each one representing the mean pixel intensity of one channel. Shaded regions represent the standard deviation across all traces

D) Five alternative sigma factor species and the housekeeping σ^A, all coupled through competition for limiting core RNAP, were simulated. Shown are sample traces for the five alternative sigmas and their cognate species. Stochastic ligand bursts were driven by a gamma distributed Ornstein-Uhlenbeck process (top left panel). Other panels show the indicated species over time for the same simulation.

Figure 2.S6

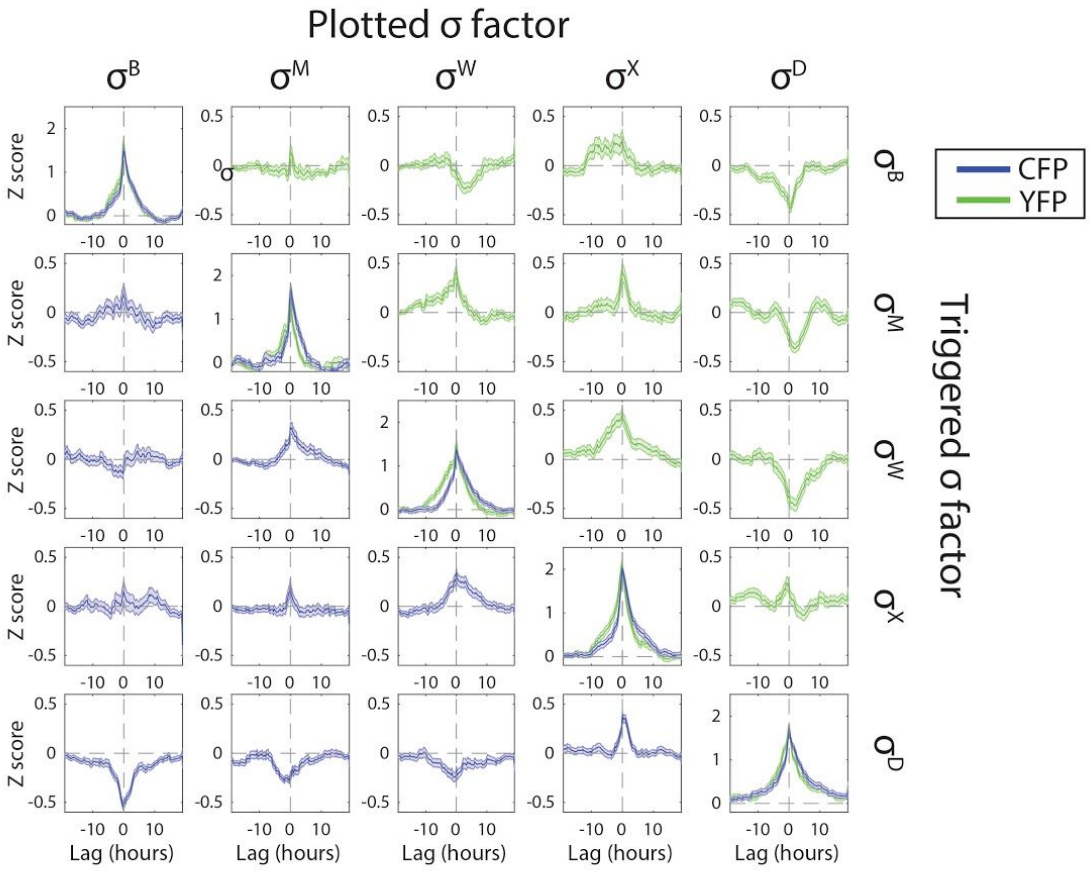

Figure 2.S6. Pulse Triggered Averaging reveals dynamic correlations between sigma factors. In this technique, pulses of one sigma factor (the 'trigger' sigma) are identified and the dynamics of a second sigma factor in the same cell are averaged in time windows around those events (STAR Methods). The resulting pulse-triggered averages are plotted here. Each pair of sigma factors is plotted twice, once triggered on the CFP trace (green), and once on the YFP trace (blue). Note the similarity in the sign of the correlation as well as the symmetry in the time delay relative to zero lag. Error bars are s.e.m. Each plot represents the average of at least 75 pulses. The underlying data set is the same as that used to calculate the cross-correlation functions (Fig. 5A).

2.6 Assessing sigma factor correlation with RNA FISH

2.6.1 Introduction

Here I describe my efforts to use RNA Fluorescence In Situ Hybridization (FISH) to answer whether pairs of sigma factors are anti-correlated in their activities. Anti-correlation between sigma factors, as described previously in this chapter, is a central component of timesharing.

I will start by describing the historical context for these FISH experiments. I had previously measured correlations between sigma factor activities using the 'matrix' of fluorescent reporter strains, where each strain reports on 2 alternative sigma factors using yfp and cfp (this is the same matrix described in this chapter). These matrix strains were grown in liquid culture with 40 μg/ml Mycophenolic Acid (MPA), and then spotted onto agarose pads for microscopy. Quantification of the fluorescent signals revealed that sigma factors did not reveal any anti-correlation.

However, the absence of anti-correlation was not definitive. There is an an important limitation to this experiment, which is that the yfp and cfp proteins are stable. This stability could lead to obscuring of any weak negative correlations. To illustrate, let us consider the following scenario: Consider 2 sigma factors σ^1 and σ^2, where they drive yfp and cfp expression respectively. And let's say that a σ^1 pulse was immediately followed by a σ^2 pulse, where importantly the two pulses do not overlap. The σ^1 and σ^2 pulses lead to production of yfp and cfp protein. But since these are 2 proteins are stable, they hang around in the cell even when their respective pulses that generated have since ceased, meaning this cell has both high yfp and cfp signal even though the underlying σ^1 and σ^2 pulses did not overlap at all. In retrospect, this caveat would be much more convincing with mathematical modeling to demonstrate the

plausibility of this effect. Although the intuition behind this caveat is quite believable, whether the caveat would have strong enough effects to erase underlying negative correlation would be better demonstrated with a model.

Yet this was the caveat that led to the birth of the RNA FISH experiments. The key idea in these experiments is that transcripts in bacteria are relatively unstable, with a half-life of ~5-10 minutes. In addition, RNA FISH can quantify at least 4 different kinds of transcripts per cell by using different fluorescent dyes, and even hundreds of transcripts with multiplexing.

2.6.2 Results

The first step in this subproject was to establish the RNA FISH protocol in *B. subtilis*. Although this protocol has previously been described in *B. subtilis*, many protocols leave out key details and thus are difficult to execute from scratch. Yet after many months and several people's help, we were able to successfully run RNA FISH in our *B. subtilis* strains (Figure 2.6.1)

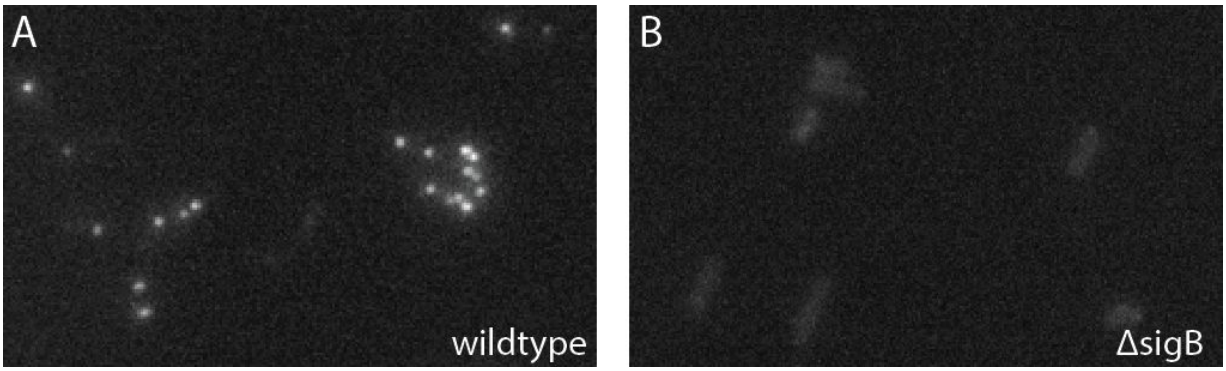

Figure 2.6.1. FISH specifically detects *sigB* transcript. (A) FISH signal from cells hybridized with probes that target *sigB* mRNA. (B) FISH signal from *ΔsigB* cells hybridized with probes that target *sigB* mRNA. Both panel images are set to the same greyscale contrast. The cells in panel B have some minimal, diffuse signal which is consistent with autofluorescence. *B. subtilis* cells grown in minimal media plus 40 μg/ml MPA to activate σ^B.

FISH probes were linked to Alexa 647.

Using this protocol, we next asked whether σ^B and σ^W activities are anti-correlated when assayed by FISH. To answer this question, we took the matrix strain 'P_B-cfp,P_W-yfp' and grew it in SMM plus 40 μg/ml MPA. Then we ran the FISH protocol to measure the *cfp* and *yfp* transcripts levels, which respectively reflect σ^B and σ^W activity (Figure 2.6.2).

The resulting data were quantified by first automatically segmenting individual cells on the phase channel images. From each cell, we quantified the transcript levels by taking the difference between the 95th percentile pixel brightness and the 50th percentile pixel brightness in the cell. We visually confirmed that this metric reflects the total number of transcripts per cell. The resulting scatter plot had a characteristic 'L-shape', suggesting that σ^B and σ^W do not typically pulse together (Figure 2.6.2B). To answer statistically whether σ^B and σ^W are in fact anti-correlated, we employed the Fisher Exact Test, which is a categorical statistical test that can assess anti-correlation. When we applied it, however, we found that no evidence of anti-correlation (Figure 2.6.2B).

The intuition behind this result can be found in the low frequency effect. The scatter in Figure 2.6.2B contains very few points in the upper right quadrant, where the upper right quadrant represents cells that are pulsing in both sigmas. However, the *expected* number of points in the upper right is *also* very low, the frequency of high signal points in either sigma is very low. So although we don't see many cells pulsing together, we don't expect that many cells anyway. One might argue that the statistical power of the test is then low. However, the number of cells assayed in (Figure 2.6.B) is ~40,000. I argue that 40,000 cells is a sufficient number to assay for this potential effect.

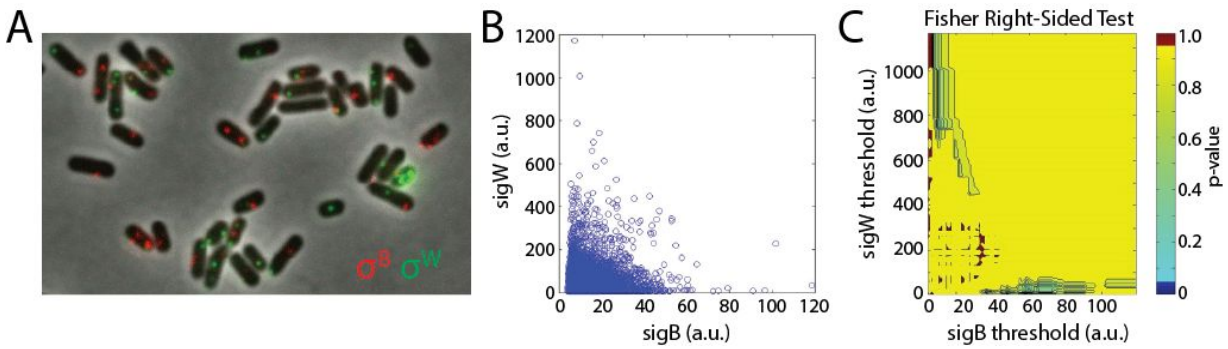

Figure 2.6.2. σ^B and σ^W activity are not anti-correlated when assayed with FISH. (A) Sample image from FISH against *cfp* and *yfp* transcripts in the matrix strain 'P_B-cfp,P_W-yfp'. We probed against the fluorescent reporter transcripts rather than the endogenous *sigB* and *sigW* transcripts, since the *cfp* and *yfp* transcripts represent more pure reporters of σ^B and σ^W activity, respectively. The *cfp* and *yfp* probes were bound to Alexa 555 and Alexa 647, respectively. (B) Scatter plot of single cell σ^B and σ^W activity as measured by FISH. Each circle in the scatter represents a single cell. The signal from each cell was quantified by taking the difference between the 95th percentile pixel brightness and the 50th percentile pixel brightness in the cell. There are ~40,000 cells in the scatter. (C) P-values from a right-sided Fisher exact test are plotted. We ran the on the Fisher exact test on the data in panel B. To run this test, we needed to first define 4 quadrants on the scatter plot, where the 4 quadrants are defined by a horizontal boundary and a vertical boundary. We then counted the number of points in each quadrant, and ran these counts through the Fisher exact test, which yielded a p-value. However, there are many choices for how to define the vertical and horizontal boundaries. To account for all possible boundary choices, we ran the Fisher test for a 2-d dimensional matrix of boundary choices. Thus each point in the panel C represents the choice of vertical and horizontal boundary, and the color of that point is the resulting p-value. Importantly, virtually none of the p-values are below 0.05.

We next wondered whether the transcriptional burstiness combined with the short half-life of transcripts could be obscuring our assay for negative correlation. To control for this possibility, we ran the FISH experiment on the matrix strain 'P_W-cfp,P_W-yfp'. If burstiness is not playing a major role, then we expect *cfp* and *yfp* transcripts levels to be well correlated with each other. However, we observed cells high in *cfp* signal but low in *yfp* signal, and vice-versa (Figure 2.6.3).

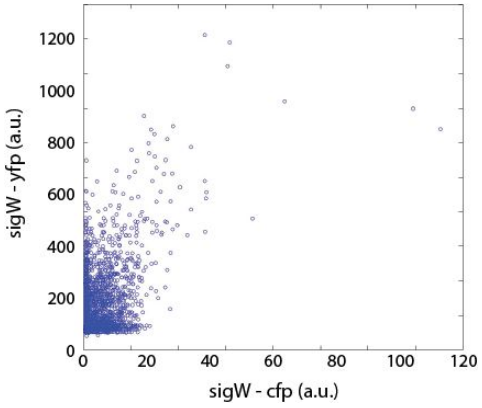

Figure 2.6.3. Transcripts of *cfp* and *yfp* are not well correlated when when driven by σ^W. (A) Scatter plot from FISH against *cfp* and *yfp* transcripts in the matrix strain 'P_W-cfp,P_W-yfp'. Each circle in the scatter represents a single cell, whose coordinate are determined by its *cfp* and *yfp* transcript levels. Transcript levels were quantified by taking the difference between the 95th percentile pixel brightness and the 50th percentile pixel brightness in the cell. Since cfp and yfp transcription are driven by the same sigma, we expect their respective transcript levels to be well-correlated. In the scatter plot, this would manifest as all dots lying on a diagonal line. However, there exist points in the scatter than are high in *cfp* but low in *yfp*, and vice versa.

This lack of correlation raised the possibility that any negative correlation could be obscured. For instance, let us consider a cell that is pulsing in σ^1 but not in σ^2. This is a cell exhibiting anti-correlated sigma activity. But assayed by FISH, it's possible the σ^1 signal would appear 'off', and the σ2 signal would also be off. Thus FISH would tell us this cell is off in both signals. By reducing the number of anti-correlated cells and increasing the number of cells in which both signals are off, any underlying negative correlation could be obscured. However, admittedly this argument would be more convincing with a simulation; in addition, it could also be a cell pulsing in both σ^1 and σ^2 appears to be pulsing in only one of them. In any case, we moved on to experiments with the mother machine, which for various reasons are preferable to the FISH experiment for our purposes.

2.6.3 RNA FISH Protocol

The protocol for RNA FISH in B. subtilis is described below. All other procedures not listed here were as described in this study.

General Considerations: Try to buy components that are nuclease-free, e.g. water and PBS. Many steps involve spinning cells, and removing supernatant. I try to be relatively aggressive in removing the supernatant since we are working with relatively small volumes. FISH probes from Stellaris and the Alexa series dyes have worked well for us. Many thanks to Timur Zhiyentayev, on whose protocol this document is heavily based.

Selected Reagents and Product Numbers

70% HB Buffer: 1 part dextran sulfate, 2 part Nuclease-Free H_2O, and 7 part formamide, all by mass
35% HB Buffer 1 part dextran sulfate, 5.5 part Nuclease-Free H_2O, and 3.5 part formamide, all by mass

Above 2 solutions can be kept at -20 C for a few months.

Lysozyme http://www.epibio.com/enzymes/lysozymes/ready-lyse-lysozyme-solution, store at -20 C
Dextran Sulfate Sigma D4911
Formaldehyde polysciences.com, #18814

Cell Preparation

Grow 10 ml of cells in orbital shaker until OD ~0.3

Fix cells

Add 5.5% formaldehyde directly to your culture flask, s.t. the final formaldehyde concentration is 0.5%

For instance, if your culture volume is 10 ml, then add 1 ml of 5.5% formaldehyde

5.5% Formaldehyde solution is diluted from 16% stock solution using PBS

Mix culture by shaking the flask by hand, I generally avoid vortexing in case this affects the cell internal state

Spin down cells, 2.5 min at 6000 rcf --> Remove supernatant --> Resuspend pellet in 1 ml 0.02 SSC. Use pipet to resuspend pellet

Spin down cells, 2.5 min at 6000 rcf --> Remove supernatant --> Resuspend cells in 200 µl of MAAM (4:1 methanol/acetic acid mixture by volume). Use pipet to resuspend pellet.

MAAM can be kept at -20 C.

Cells can be kept in MAAM at -80 C for 1-2 days without loss in RNA hybridization efficiency.

Cell Hybridization and Washing

Spin cell suspension(50-100 µl), remove sup, and resuspend thoroughly in 50 µl of 70% hybridization buffer.

Heat for 1 hr at 65 C to denature target nucleic acid. (not necessary for RNA FISH, may be necessary for DNA FISH)

You may want to test this step for yourself.

Spin down cells in tabletop centrifuge, remove sup, and replace 70% hybr buffer with 100 µl of lysozyme for 10 min at RT.

Consider 35,000 U/µl stock solution from Epicentre to be 100X.

Dilute 100X solution to 2X using 0.02 SSC.

Spin down cells in tabletop centrifuge, remove sup, add 50 µl of 70% hybr buffer. Then add 50 µl of 35% hybr buffer. Mix using Pipet Tip

Add 1 µl of probe solution, and resuspend cells using pipet.

Wrap tube in foil, incubate at 37 C on orbital shaker for 3 hrs. Then Image!

2.7 Materials and Methods

2.7.1 Table of Strains and Plasmids

Identifier	**Plasmid**	**Source**	**Identifier**
Plasmid 1	ppsB::P_{trpE}-mCherry ErmR	This work	Plasmid 1
Plasmid 2	sacA::$P_{?}$-yfp CmR	This work	Plasmid 2
Plasmid 3	amyE::$P_{?}$-3Xcfp SpectR.	This work	Plasmid 3
Plasmid 4	amyE::$P_{hyperspank}$-sigB SpectR	This work	Plasmid 4
Plasmid 5	pyrD::P_{B}-cfp kanR	This work	Plasmid 5

ID	**Bacterial Strain Genotype**	**Construction/Source**
PY79	*trpC2 (this genotype omitted in derived strains, below)*	BGSC 1A776
JP1	*ppsB::P_{trpE}-mCherry* PhleoR	[68]
JP2	JP1;ytvA::NeoR	JJB751→JP1 (NeoR selection)[68]
JP3	JP2;sacA::P_{B}-yfp CmR	Plasmid (2)→JP2
JP4	JP2;sacA::P_{M}-yfp CmR	Plasmid (2)→JP2
JP5	JP2;sacA::P_{W}-yfp CmR	Plasmid (2)→JP2
JP6	JP2;sacA::P_{X}-yfp CmR	Plasmid (2)→JP2
JP7	JP2;sacA::P_{D}-yfp CmR	Plasmid (2)→JP2
JP8	JP2;sacA::P_{L}-yfp CmR	Plasmid (2)→JP2
JP9	JP2;sacA::P_{Y}-yfp CmR	Plasmid (2)→JP2
JP10	JP2;sacA::P_{A}-yfp CmR	Plasmid (2)→JP2
JP11	JP3;rsbU-rsbX::TetR	[68] [68]
JP12	JP4; sigM::TetR	[69]
JP13	JP4; sigW::ErmR	[69]
JP14	JP6;sigX::SpectR	[70]
JP15	sigD::TetR	[71,72]
JP16	JP7; sigD::TetR	JP15→JP7 (TetR selection)
JP17	JP1; sacA::P_{L}-yfp CmR	JP8→JP1 (CmR selection)
JP18	JP17;sigL::KanR	[29]

JP19	JP1; sacA::P_Y-yfp CmR	JP9→JP1 (CmR selection)
JP20	JP19;sigY::KanR	[73]
JP21	JP3;amyE::P_B-3Xcfp SpectR	Plasmid (3)→JP3
JP22	JP3;amyE::P_M-3Xcfp SpectR	Plasmid (3)→JP3
JP23	JP3;amyE::P_W-3Xcfp SpectR	Plasmid (3)→JP3
JP24	JP3;amyE::P_X-3Xcfp SpectR	Plasmid (3)→JP3
JP25	JP3;amyE::P_D-3Xcfp SpectR	Plasmid (3)→JP3
JP26	JP4;amyE::P_B-3Xcfp SpectR	Plasmid (3)→JP4
JP27	JP4;amyE::P_M-3Xcfp SpectR	Plasmid (3)→JP4
JP28	JP4;amyE::P_W-3Xcfp SpectR	Plasmid (3)→JP4
JP29	JP4;amyE::P_X-3Xcfp SpectR	Plasmid (3)→JP4
JP30	JP4;amyE::P_D-3Xcfp SpectR	Plasmid (3)→JP4
JP31	JP5;amyE::P_B-3Xcfp SpectR	Plasmid (3)→JP5
JP32	JP5;amyE::P_M-3Xcfp SpectR	Plasmid (3)→JP5
JP33	JP5;amyE::P_W-3Xcfp SpectR	Plasmid (3)→JP5
JP34	JP5;amyE::P_X-3Xcfp SpectR	Plasmid (3)→JP5
JP35	JP5;amyE::P_D-3Xcfp SpectR	Plasmid (3)→JP5
JP36	JP6;amyE::P_B-3Xcfp SpectR	Plasmid (3)→JP6
JP37	JP6;amyE::P_M-3Xcfp SpectR	Plasmid (3)→JP6
JP38	JP6;amyE::P_W-3Xcfp SpectR	Plasmid (3)→JP6
JP39	JP6;amyE::P_X-3Xcfp SpectR	Plasmid (3)→JP6
JP40	JP6;amyE::P_D-3Xcfp SpectR	Plasmid (3)→JP6
JP41	JP7;amyE::P_B-3Xcfp SpectR	Plasmid (3)→JP7
JP42	JP7;amyE::P_M-3Xcfp SpectR	Plasmid (3)→JP7
JP43	JP7;amyE::P_W-3Xcfp SpectR	Plasmid (3)→JP7
JP44	JP7;amyE::P_X-3Xcfp SpectR	Plasmid (3)→JP7
JP45	JP7;amyE::P_D-3Xcfp SpectR	Plasmid (3)→JP7
JP46	JJB213; rsbU-rsbX::TetR	[68]
JP47	JP1 ; rsbU-rsbX::TetR	JP46→JP1 (TetR selection)
JP48	JP47; amyE::$P_{hyperspank}$-sigB Spect	Plasmid (4) above→JP47
JP49	JP48; pyrD::P_B-cfp KanR	Plasmid (5)→JP48

JP50	JP49; sacA::P_W-yfp CmR	Plasmid (2)→JP49
JP51	JP49; sacA::P_D-yfp CmR	Plasmid (2)→JP49
JP52	JP50; hag::ErmR	BGSC BKEHAG→JP50[74]
JP53	JP51; hag::ErmR	BGSC BKEHAG→JP51[74]
JP54	JP11;hag::ErmR	BGSC BKEHAG→JP26 [74]
JP55	JP16;hag::ErmR	BGSC BKEHAG→JP26 [74]
JP56	JP21;hag::ErmR	BGSC BKEHAG→JP31 [74]
JP57	JP26;hag::ErmR	BGSC BKEHAG→JP36 [74]
JP58	JP31;hag::ErmR	BGSC BKEHAG→JP41 [74]
JP59	JP17;hag::ErmR	BGSC BKEHAG→JP27 [74]
JP60	JP22;hag::ErmR	BGSC BKEHAG→JP32 [74]
JP61	JP27;hag::ErmR	BGSC BKEHAG→JP37 [74]
JP62	JP32;hag::ErmR	BGSC BKEHAG→JP42 [74]
JP63	JP23;hag::ErmR	BGSC BKEHAG→JP33 [74]
JP64	JP28;hag::ErmR	BGSC BKEHAG→JP38 [74]
JP65	JP33;hag::ErmR	BGSC BKEHAG→JP43 [74]
JP66	JP29;hag::ErmR	BGSC BKEHAG→JP39 [74]
JP67	JP34;hag::ErmR	BGSC BKEHAG→JP44 [74]
JP68	JP35;hag::ErmR	BGSC BKEHAG→JP45 [74]

2.7.2. Strain and Plasmid Construction

Bacillus subtilis Strains were from the PY79 genetic background, and the list of strains used is given in the Key Resources Table. Many starting strains/genomic DNA were kind gifts of C.W. Price (see references below), and many sigma factor deletion strains were kind gifts from John Helmann. Several strains were obtained from the Bacillus Genetic Stock Center (BGSC), and their strain codes are noted in the Key Resources Table.

In above table, in the column labeled "Construction Procedure", the '→' symbol indicates an integration event from plasmid or genomic DNA into the strain after the arrow. For example, in strain JP2, the construction procedure is listed as "*JJB751→JP1 (with Neo^R selection)*", meaning that the genomic DNA of JJB751 was prepared and transformed into JP1 with selection on neomycin.

Antibiotic resistance was switched using a previously described antibiotic switching vector system [71]. Deletions were made by replacing genes of interest with a selection marker via a linear DNA fragment homologous to the region of interest.

All plasmids were cloned using *E.coli* strain DH5α and a combination of standard molecular cloning techniques and non-ligase dependent cloning using Clontech In-Fusion Advantage PCR Cloning kits. Plasmid constructs were integrated into *B. subtilis* chromosomal regions via double crossover using standard techniques. The following list provides a description of each plasmid constructed, with details on integration position/cassette and selection marker given at the beginning. Note that all plasmids below replicate in *E. coli* but not in *B. subtilis*.

Plasmid list:

1) *ppsB::P_{trpE}-mCherry Erm^R* - This plasmid was used to provide uniform expression of mCherry from a σ^A-dependent promoter, enabling automatic image segmentation (cell identification) in time-lapse movie analysis. A minimal σ^A promoter was used from the *trpE* gene and cloned into a vector with *ppsB* homology regions [68]. The original integration vector was a gift from A. Eldar [75]. For some strains, the selection marker was subsequently changed, in *B. subtilis,* to either *Kan^R* or *Phleo^R*.

2) *sacA::$P_?$-yfp Cm^R* - Target promoters of each alternative sigma factor, ? = B, D, L, M, W, X, Y, A were cloned into the EcoRI/BamHI sites of AEC127 [75]. For σ^A, a minimal σ^A promoter was used from the *trpE* gene[68]. Target promoter sequences for alternative sigmas are described in a later section.

3) *amyE::P$_?$-3Xcfp Spect^R*. Target promoters of each alternative sigma factor, ? = B, D, L, M, W, X, Y, were cloned into the EcoRI/Nhe1 sites of plasmid amyE::3XCFP *Spect^{R68}*. This plasmid, based on pDL30, contains 3 separate copies of *cfp*, each with its own RBS. Target promoter sequences are described in a later section.

4) *amyE::P$_{hyperspank}$-sigB Spect^R* - The coding region of sigB, along with a 5' transcriptional terminator, was cloned behind the $P_{hyperspank}$ IPTG-inducible promoter in plasmid pDR-111 (gift of D. Rudner, Harvard).

5) *pyrD::P$_B$-cfp kan^R*. Target promoter of σ^B, followed by the CFP fluorescent protein gene, was cloned into the EcoRI/BseRI site of the ECE171 plasmid [76].

Target Promoters for Sigma Factors

Below is a list of the promoters used to report on each sigma factor's activity. Each sequence below contains a binding site for the given sigma factor, and were cloned into the requisite targeting plasmid. Note restriction enzyme sites are *not* included in the displayed sequences.

1) σ^B : Sequence was chosen from the σ^B binding site upstream of the *rsbV* gene [77,78].

5'-GTTTCTTGGAGCGTCCTGATCTGCAGAAGCTCATTGAGGAACATATGTGTTCCTCTGCGCAGGAAATGGTCAAA
AACATTTATGACAGCCTCCTCAAATTGCAGGATTTTCAGCTTCACGATGATTTTACGTTAATTGTTTTGCGGAGAAA
GGTTTAACGTCTGTCAGACGAGGGTATAAAGCAACTAGTGATTTGAAGGAAAATTTG - 3'

2) σ^D: Sequence was chosen from the σ^D binding site upstream of the *flgB* gene [79]

5' – TTTTGCATTTTTCTTCAAAAAGTTTCAAAAATGCCGAAAAGAAAGGAGAAAAAACAGAAATTCTG –3'

3) σ^L: Sequence was chosen from the σ^L binding site upstream of the *ptb* gene [33].

5'-

AATATGGCCTTGCAAATGAAGGCATGCAATAATTTGCAGAATAAACGCAAACATCTGCACGAATGTTTCGGTATAC

CTGGTATGACAGCACCCTTAAGAGCTGGCATGGAACTTGCATAATAAAAGGCGGAG – 3'

4) σ^M: Sequence was chosen from the σ^M binding site upstream of the *sigM* gene [80].

5' – TTTGCATGTAATGTGCAACTTTAAACCTTTCTTATGCGTGTATAACATAGAGG-3'

5) σ^W: Sequence was chosen from the σ^W binding site upstream of the *ydbS* gene [81].

5' – TTAAGAATGAAACCTTTCTGTAAAAGAGACGTATAAATAACGACGAAAAAAAG – 3'

6) σ^X: Sequence was chosen from the σ^X binding site upstream of the *sigX* gene [82].

5' – TTGTAATGTAACTTTTCAAGCTATTCATACGACAAAAAAGTGAACGGAGGG – 3'

7) σ^Y: Sequence was chosen from the σ^Y binding site upstream of the *sigY* gene [73].

5' – GAATTGTAAAAAAGATGAACGCTTTTGAATCCGGTGTCGTCTCATAAGGCAGAAAAACA – 3'

2.7.3. Microscopy and Sample Preparation

All data were acquired using a CoolSnap HQ2 camera attached to a Nikon inverted TI-E microscope, equipped with the Nikon Perfect Focus System (PFS) hardware autofocus module. Molecular Devices commercial software (Metamorph 7.5.6.0) controlled microscope, camera, motorized stage (ASI instruments), and epifluorescent and brightfield shutters (Sutter Instruments). For experiments in liquid culture and agarose pads, epi-illumination was provided by a 300 W Xenon light source (LamdbaLS, Sutter instruments) connected via a liquid light guide into the illuminator of the scope. Between days, relative lamp intensity levels were monitored by taking an image of fluorescent beads and measuring their

mean intensity. Exposure times were then adjusted to keep per exposure light levels constant between experiments. For experiments in the mother machine, epi-illumination was provided by a solid state white light source (Lumencor SOLA, Lumencor SOLA). Phase contrast illumination was provided by a halogen bulb to allow verification of cell focus and cell shape. Temperature control was achieved using an enclosed microscope chamber (Nikon) attached to a temperature sensitive heat exchanger set to 37 °C. All experiments used a Phase 100x Plan Apo (NA 1.4) objective. Chroma filter sets used were as follows: #41027 (mCherry), #41028 (YFP), and #31044v2 (CFP). The interval between consecutive imaging was 15 minutes.

Unless otherwise noted, cells were grown in Spizizen's minimal media, or SMM [83], which uses 0.5% glucose as the carbon source, and tryptophan (50 μg/ml) as an amino-acid supplement. Mycophenolic acid (MPA) was dissolved in DMSO and diluted 1000 fold into working concentrations in liquid and pad conditions. IPTG was dissolved in H_2O and diluted 1000 fold into working concentrations. Concentrations of 0.1% DMSO were not found to affect cell growth or σ^B activity.

Samples were prepared following a time-lapse microscopy protocol described previously[84]. A stab from a glycerol stock was inoculated into SMM, placed into a 30 C shaking incubator, and grown overnight. Cells were then diluted back to a final concentration of 0.01 OD_{600} in a total volume of 2 ml of SMM. Cells were then grown in a 37 °C shaker for 3 hours.

For liquid culture experiments, MPA (MP Biomedicals cat #194172) was then added to the culture to a final concentration for 40 μg/ml. Cells were returned the 37 °C shaker for 3 hours, after which 2 μl of culture was spotted onto an agarose pad. Agarose pads were constructed of 1.5% low melt agarose solution in PBS, and then imaged.

For time-lapse movies, cells were spotted on solidified 1.5% low melt agarose in SMM pads. MPA was also added to the pads to final concentration of 40 μg/ml. These prepared pads were then enclosed in coverglass bottom dishes (Wilco #HBSt-5040), sealed with parafilm or grease to prevent evaporation, and then imaged.

Sample preparation for stationary-phase (conditioned medium) experiments

Conditioned medium was prepared growing PY79 wild-type B. subtilis strain in 2 ml of LB at 37 °C for 4.5h. Then, this culture was diluted in 23 ml of fresh LB and was grown at 37 °C for 17.5h. After this, cells were removed by centrifugation (at 5000 rpm for 10 min) and the supernatant was sterilized by filtration (using 0.2 μm pore-size filters) and stored at −80 °C. This conditioned media protocol was defined previously [85].

Cells were grown from glycerol stocks in LB until OD_{600} 1.5-3.5, then diluted back into LB (1:10) in PBS to an OD_{600} of 0.05. This culture was grown at 37 °C for a minimum of 4 hours and a maximum of 7, when cells were diluted to an OD_{600} of 0.8-0.1 with conditioned medium (1:45) in PBS for imaging. 1.5% low melting agarose pads were prepared with conditioned medium (1:45) in PBS. After allowing cells to equilibrate for 2-3 hours, time-lapse acquisition was started.

Sample preparation for Mother Machine Experiments

Wafer Construction

Silicon wafers were constructed using photolithography by Shivakumar Bhaskaran at the Searle CleanRoom Manager at the University of Chicago. The CAD file for the design was a kind gift from Richard Losick and Johan Paulsson [86].

Chip Construction

Mother machine chips were constructed by first mixing Sylgard 184 (Dow Corning) Parts A and B in ratios of 10 to 1 by weight, respectively. Both parts were thoroughly mixed together, and then degassed in a vacuum chamber (Welch 256413-01) for 1 hr or until there was no visual sign of bubbles. The PDMS mixture was poured onto a wafer that had been placed into a 'boat' of aluminum foil, then baked at 65 °C overnight. The solidified PDMS was then carefully peeled off the wafer, cut with a scalpel to isolate the device, and fluidic inlets and outlets were created with with a 0.5 mm diameter hole punch (World Precision Instruments).

Chip Bonding to Coverslip

Glass coverslips (#1.5 Gold Seal 3416) were cleaned by sonicating in an Isopropanol Bath for 30 minutes, then sonicating in deionized water 3 times for 30 min. The microfluidic chips were cleaned simply by applying and removing Scotch tape multiple times. Chips were bonded using a plasma cleaner (Autoglow) with an attached O_2 tank, at 50 W for 6 seconds, and was performed at the Micro Nano Fabrication Laboratory at Caltech. The chip-coverslip complex was then baked at 85 °C overnight. Importantly, we found using O_2 with the plasma cleaner strengthened the bond between the glass coverslip and PDMS chip.

Cell preparation and Cell Loading onto Chip

Cells were grown from glycerol stocks in SMM at 30 °C overnight. Cells were diluted to 0.01 OD_{600} in the morning, and then grown for 3 hours at 37 °C. MPA was then added to a final concentration of 40 μg/ml, and then the culture was grown at 37 °C for another 6 hours. Cells were then pipetted into the chip inlet by utilizing gel loading tips (Molecular BioProducts 2155). To ensure cell entry into the narrow side channels of the chip, the entire coverslip and chip assembly was placed into a custom adapter [86], and then spun in a tabletop microcentrifuge (Eppendorf 5424R) for 10 min at 3000 rcf.

Fluidic inlet and outlets

Fluid flow was driven by a syringe pump (NE-1600, syringepumps.com), which can drive up to six 10-ml syringes (BD 309604) in parallel. Unless otherwise noted, we used a flow rate of 1.5 μl/min. We used Tygon tubing (Saint Gobain AAD04103) for all tubing purposes. A blunt end needle (McMaster-Carr 75165A681) interfaced between the syringe and the tubing, and the same blunt end needle (with luer lock tip removed) interfaced between the tubing and the chip.

Media driven by the syringe

Unless noted otherwise, the media used in the mother machine was SMM, supplemented with i and 100 μg/ml BSA (Sigma A7906).

The exception was the competition assay in the mother machine. Syringes were initially loaded with the media as described above, namely SMM + 40 μg/ml MPA + 100 μg/ml BSA. But in the middle of acquisition, they syringes were switched to new syringes that contained the same media, excepted supplemented with additional 1 mM IPTG.

Mother Machine Microscopy

The coverslip/chip apparatus with attached fluidic inputs and outputs was fixed to the microscope stage insert (I-3014, ASI Imaging) using lab tape, and then imaged as described in the Microscopy section.

Competition Assay in the Mother Machine

Cells were loaded into the mother machine as described above.

Multiple σ factor simulation

We constructed a model to simulate the activity of five identical, independent σ factor pathways, interacting only through their association with shared RNA polymerase core (R). The main features of the model are:

- Transcriptional autoregulation. Each sigma factor comprises an operon containing the σ factor (S_i, where i = 1, 2, … 5) and its cognate anti-σ factor (A_i). This operon is activated by its own σ factor. A sixth σ factor with no anti-σ is considered, representing the housekeeping factor σ^A.
- Inhibition by a co-expressed anti-σ factor. The σ factor binding to its cognate anti-σ prevents it from associating with RNAP.
- Limiting levels of RNAP resulting in competitive binding between σ factors.
- A ligand that sequesters its cognate anti-σ. A common feature among extra-cytoplasmic (ECF) sigma factors is that in most cases the anti-σ is a transmembrane protein that only releases its cognate sigma factor when it receives a certain input from the extracellular environment [87]. Hence, we implemented a ligand (L_i) in our model responsible for sequestration of its cognate anti-σ to allow for the release of the corresponding σ factor.

This minimal structure is sufficient to generate pulses in the σ·RNAP complex concentration that cause the alternative sigma factors to time-share core RNAP.

An additional equation (equation S2, below) simulates σ^A, the main - or housekeeping - σ factor. Its structure resembles that of the alternative σ factors, but without an anti-σ factor or corresponding ligand. The removal of the anti-σ factor results in a non-pulsatile and constitutive σ^A·RNAP concentration.

The transcription terms for σ factors and anti-σ factors are assumed to be linear, as are all degradation terms. The positive transcriptional regulation is modeled with Michaelis-Menten kinetics. σ^A is assumed to be expressed at a level larger than the alternative σ factors, thus effectively avoiding competing with them. Negative regulation occurs by way of sequestration, with linear rates for complex association and

dissociation. Importantly, the sigma-RNAP complex produces more anti-sigma than sigma, a feature consistent with experimental measurements[88]. This relative advantage in anti-sigma production allows anti-sigma levels to 'catch up' to sigma levels and terminate the pulse. The ligand concentration was generated in bursts distributed randomly and uniformly over time, and exponentially distributed in magnitude. This was motivated by previous observations [89–91] that cellular protein concentrations follow a gamma distributed Ornstein-Uhlenbeck (GOU) process. This implementation allows for independent manipulation of burst size and frequency. To optimize computational efficiency, ordinary (not stochastic) differential equations were solved between the stochastic ligand bursts in the discretized stochastic GOU process.

The following ODEs describing the dynamics for each species and their complexes were solved numerically in MATLAB using a variable step BDF method (http://www.mathworks.co.uk/help/matlab/ref/ode15s.html). Parameters can be found in the table below. The MATLAB codes for the model simulation and analysis are available upon request.

Alternative σ factors (S_i):

transcription + positive auto-regulation + complex dissociation + complex association + degradation

$$\frac{d[S]_i}{dt} = \alpha_s + \beta_s[RS]_i + k_{rs-}[RS]_i + k_{sa-}[SA]_i - k_{rs+}[R][S]_i - k_{sa+}[S]_i[A]_i - \delta_s[S]_i \quad \text{(S1)}$$

Housekeeping σ factor (S_A):

transcription + positive auto-regulation + degradation

$$\frac{d[S]_A}{dt} = \alpha_{sA} + \beta_{sA}[RS]_A + k_{rsA-}[RS]_A - k_{rsA+}[R][S]_A - \delta_{sA}[S]_A \quad \text{(S2)}$$

Anti-σ factors (A_i):

transcription + up-regulation + complex dissociation – complex association – degradation

$$\frac{d[A]_i}{dt} = \alpha_a + \beta_a[RS]_i + k_{sa-}[SA]_i + k_{al-}[AL]_i \quad \text{(S3)}$$

$$- k_{sa+}[S]_i[A]_i - k_{al+}[A]_i[L]_i - \delta_a[A]_i$$

RNA polymerase · σ factor complex (RS):

complex association – complex dissociation – degradation

$$\frac{d[RS]_i}{dt} = k_{rs+}[R][S]_i - k_{rs-}[RS]_i - \delta_{rs}[RS]_i \quad \text{(S4)}$$

RNA polymerase · σ^A complex (RS_A):

complex association – complex dissociation – degradation

$$\frac{d[RS]}{dt} = k_{rsA+}[R][S]_A - k_{rsA-}[RS]_A - \delta_{rsA}[RS]_A \quad \text{(S5)}$$

Anti-σ factor · σ factor complex (SA):

complex association – complex dissociation – degradation

$$\frac{d[SA]_i}{dt} = k_{sa+}[S]_i[A]_i - k_{sa-}[SA]_i - \delta_{sa}[SA]_i \quad \text{(S6)}$$

Ligand (L):

complex dissociation – complex association – degradation

$$\frac{d[L]_i}{dt} = k_{al-}[AL]_i - k_{al+}[A]_i[L]_i - \delta_l[L]_i \quad \text{(S7)}$$

Anti-σ factor · ligand complex (AL):

complex association – complex dissociation – degradation

$$\frac{d[AL]_i}{dt} = k_{al+}[A]_i[L]_i - k_{al-}[AL]_i - \delta_{al}[AL]_i \quad \text{(S8)}$$

The free amount of RNAP is given by the conservation law

$$[\ R\ ] = R_{tot} - \sum_i [RS]_i \quad \text{(S9)}$$

where the sum runs over all sigma factors, including the housekeeping sigma factor.

Finally, the dynamics of the ligands are modified by adding the random quantity ε_0 (exponentially distributed) at random times T_0 (uniformly distributed) throughout the simulation.

$$L(t) \rightarrow L(t) + \varepsilon_0\, \mathrm{L(t)} \quad \text{(S10)}$$

Model interactions and rate parameter values.

Reaction	Parameter	Description	Reactant(s)	Value
Basal transcription	α_s	Basal rate	alternative σ factor	1.5 nM/min
	α_{sA}	Basal rate	housekeeping σ^A factor	180 nM/min
	α_a	Basal rate	anti-σ factor	0.6 nM/min
Up-regulation	β_s	Transcription rate	alternative σ factor	0.06 min^{-1}
	β_{sA}	Transcription rate	σ^A	$6\times10^{-4}min^{-1}$
	β_a	Transcription rate	anti-σ factor	0.09 min^{-1}
Association	k_{rs+}	Binding rate	RNAP, σ factor	0.03 $nM^{-1}min^{-1}$
	k_{rsA+}	Binding rate	RNAP, σ^Afactor	0.3 $nM^{-1}min^{-1}$
	k_{sa+}	Binding rate	σ factor, anti-σ factor	0.024 $nM^{-1}min^{-1}$
	k_{al+}	Binding rate	anti-σ factor, ligand	0.018 $nM^{-1}min^{-1}$
Dissociation	k_{rs-}	Unbinding rate	RNAP•σ factor complex	0.3 min^{-1}
	k_{rsA-}	Unbinding rate	RNAP•σ^Afactor complex	0.003 min^{-1}
	k_{sa-}	Unbinding rate	σ factor•anti-σ factor complex	0.06 min^{-1}
	k_{al-}	Unbinding rate	anti-σ factor•ligand complex	0.03 min^{-1}
Degradation	δ_s	Degradation rate	alternative σ factor	0.0167 min^{-1}
	δ_{sA}	Degradation rate	housekeeping σ^A factor	0.0167 min^{-1}
	δ_a	Degradation rate	anti-σ factor	0.0167 min^{-1}
	δ_{rs}	Degradation rate	RNAP•σ factor complex	0.0167 min^{-1}
	δ_{rsA}	Degradation rate	RNAP•σ^Acomplex	0.0167 min^{-1}
	δ_{sa}	Degradation rate	σ factor•anti-σ factor complex	0.0167 min^{-1}
	δ_{al}	Degradation rate	anti-σ factor•ligand complex	0.0167 min^{-1}
	δ_l	Degradation rate	ligand	0.0167 min^{-1}
Total RNAP	R_{tot}	Concentration	RNAP	12.6μM
Burst size	ε_0	Concentration	ligand	10 μM
Burst frequency	T_0	Rate	ligand	3.33×10-3min^{-1}

2.7.4 Quantification and Statistical Analysis

Image Analysis for Liquid Culture Snapshots

Quantitative image analysis of microscopy images was performed in MATLAB as described previously [92]. Briefly, the constitutive mCherry was used as a segmentation channel, and cell edges were detected using a Laplacian of Gaussian filter. The segmentation masks identified with mCherry were then used to extract cell fluorescence values from other channels.

Image Analysis for Agarose Pad Movies

Quantitative movie analysis used custom image analysis code, namely the Schnitzcells software written in MATLAB, as described in previous work [84]. Briefly, cells were segmented on the constitutive mCherry using edge detection with a Laplacian of Gaussian filter. Cell masks were then manually corrected, tracked, and then the cell tracks were further manually corrected, all using Schnitzcells.

Image Analysis for Mother Machine Movies

Each microscope image contained multiple subchannels. We used custom MATLAB code to automatically identify subchannels, and crop them out into new image files. This was important not only to follow cells in individual subchannels, but to reduce the computational load of segmentation (described below).

Cell segmentation was accomplished using the Trainable Weka Segmentation plugin in Fiji, and was automated using a custom Beanshell script inside Fiji. We were careful to train the plugin to accurately separate adjacent cells. Cell tracking of the mother cell was done in MATLAB, where for every frame we simply took the mother cell at the 'end' of the channel. This tracking method produced accurate tracks

except in cases of cell death or flickering segmentation, where a cell very dim in mCherry could be segmented in one frame but not the next, leading to a tracking error. Next, extraction of cell fluorescence and other cell properties such as cell length were done in MATLAB.

To account for tracking errors, we used a custom Graphical User Interface (GUI) in MATLAB, based on one used previously [93]. By manually searching for obvious errors in cell length, we manually marked problematic tracks in the GUI to be excluded from any further analysis.

Promoter Activity Calculation

Calculation of single-cell promoter activity, also called σ activity, is similar to previously reported methods [68], and was calculated in the same way for both agarose pad and mother machine movies. Here we provide a brief overview of these calculations.

We are interested in finding the instantaneous rate of fluorescent protein production in individual cells. We calculate this quantity from timelapse microscopy by taking a time derivative of the fluorescent protein level in the cell. Consider a timelapse movie of a single growing *B. subtilis* cell expressing *yfp*. For the moment, let us ignore cell division, so we are simply considering the cell as it elongates along its major axis. We denote the total fluorescence of the cell $T(t)$, the *yfp* promoter activity (i.e. production rate) $P(t)$, and the photobleaching rate of *YFP* γ. Note that $T(t)$ and $P(t)$ are functions of time, and that γ includes YFP degradation as well as photobleaching, although the degradation rate is typically negligible. These variables are related to each other as follows:

$$T'(t) = P(t) - \gamma T(t)$$

Here, the $'$ symbol denotes a time derivative, and computing $P(t)$ evidently requires measurement of the time derivative $T'(t)$. Although we could try to differentiate $T(t)$ from microscopy data, this can be

sensitive to cell segmentation errors. As an alternative, we can replace $T(t)$ with $T(t) = M(t)V(t)$, where $M(t)$ is the mean fluorescence of the cell, and $V(t)$ is the cell volume. In addition, since *B. subtilis* grows lengthwise, we replace $V(t)$ with $V(t) = cL(t)$, where c is a constant and $L(t)$ is the measured cell length at time t. The value of c should be approximately equivalent to the cell's cross-sectional area, but we will omit c in further calculations, since it will only change the final values by a constant factor, and fluorescence units are arbitrary to begin with. After substituting these 2 relationships into the above equation for $T'(t)$, we can solve for $P(t)$:

$$T'(t) = P(t) - \gamma T(t)$$

$$(M(t)V(t))' = P(t) - \gamma M(t)V(t)$$

$$M'(t)V(t) + M(t)V'(t) = P(t) - \gamma M(t)V(t)$$

$$M'(t)L(t) + M(t)L'(t) = P(t) - \gamma M(t)L(t)$$

$$P(t) = M'(t)L(t) + M(t)L'(t) + \gamma M(t)L(t)$$

$$\text{Promoter activity} \equiv \frac{P(t)}{L(t)} = M'(t) + M(t)\frac{L'(t)}{L(t)} + \gamma M(t)$$

This final equation enables us to calculate the *promoter activity*, or σ *activity*, defined as $\frac{P(t)}{L(t)}$, or the production rate per unit length of the cell, in terms of observables. σ activity can be interpreted as the approximate protein production rate per chromosomal equivalent, allowing comparison of protein production through all points in the cell cycle. To compute time derivatives, the measured values of $M(t)$ and $L(t)$ were first smoothed to reduce noise (MATLAB *smooth* function with Lowess algorithm). For γ, we used a value of 0.05 as described previously [68].

Pulse Identification for Agarose Pad Movies

To automatically identify pulses from the promoter activity traces, we used custom MATLAB software [68]. The code first identified local maxima (peaks) in the traces of promoter activity vs. time. A point in the trace was deemed a peak if its height was the largest within a window of 7 frames (frames were separated by time intervals of 10-15 min depending on the movie). In other words, a peak at time t_k must have height greater than all heights at times t_{k-3} through t_{k+3}. For peaks near the start or end of the trace, the window size was decreased as necessary, e.g. a peak at timepoint t_3 was compared against t_0-t_6.

To suppress peaks arising from random fluctuations, the code utilized 2 additional parameters: 1) amplitude and 2) amplitude relative to baseline. The amplitude was defined as the height of the peak minus the average height of the 2 flanking minima surrounding the peak. The amplitude relative to baseline was defined as the height of the peak divided by the average height of the 2 flanking minima. The code rejected potential peaks whose amplitude is below the defined threshold of 7.5 arbitrary units(a.u) The code also rejected peaks whose amplitude relative to baseline was less than 0.5 a.u.. These two thresholds were chosen to avoid peak detection in timelapse data from a non-pulsatile $P_{hyperspank}$-yfp strain induced with IPTG, where the IPTG level was such that the average activity of the $P_{hyperspank}$-yfp was equal to that of the P_B-yfp strain at 40 μg/ml MPA. Note the $P_{hyperspank}$-yfp strain in movies shows only small fluctuations that are qualitatively distinct from the large pulses from the alternative sigma factor reporter strains. The results of automatic pulse detection were checked against raw data and the promoter activity traces and showed good agreement with manual identification of pulses.

Pulse Identification for Mother Machine Movies and Pulse Characteristic Calculations

Pulses were identified from promoter activity traces using MATLAB's findpeaks function, where the minpeakdistance option was set to 5 to prevent double-counting peaks, and the minpeakheight option was set to 1.7 standard deviations above the mean activity to suppress detection of small fluctuations. Pulse identification showed good agreement with manual inspection of pulses.

Pulse characteristics were also found with MATLAB's findpeaks function, which has as output options the peak widths and peak amplitudes. The average pulse shape (Figure 2C) was found by taking each pulse, subtracting its baseline, and then dividing by the amplitude. The baseline was calculated by subtracting the pulse's max value from the amplitude outputted by findpeaks. Data was pooled across

multiple matrix strains carrying the same fluorescent reporter for any given sigma factor, resulting at least 320 pulses per sigma factor. The normalized pulse amplitude distributions (Figure 2D) were calculated by first dividing each sigma's set of pulse amplitudes by its mode, and then plotted the resulting distribution function.

Cross correlation functions, Pulse Triggered Averaging, and L-plots

All figure panels for the cross correlation functions (Figure 5A), pulse triggered averages (Figure S6) and L-plots (Figure 5C) were calculated from the same underlying dataset, namely from the matrix strains grown in the mother machine. For each matrix strain, we obtained at least 73 single cell traces that typically grew for at least 30 cell cycles.

Cross correlation functions (ccf) were calculated using MATLAB's xcov function, with option 'unbiased' enabled, and was performed on mean fluorescence rather than promoter activity traces. To correct for long-term changes in sigma activity, the mean time trace was first subtracted from each trace. The ccf for each trace was calculated separately, and the resulting set of ccf's was averaged for Figure 5. Each average ccf shown was calculated from at least 73 single cell traces.

The pulse triggered average plots (Figure S6) were also calculated from mean fluorescence traces, done as follows. Each time trace of mean fluorescence was first converted to Z-scores by subtracting the mean trace and then dividing by the standard deviation. Then peaks were computationally identified for one sigma (the 'trigger' sigma), and for each peak a time window in the other sigma (the 'plotted' sigma) was extracted. Importantly,the time window was centered at exactly the peak in the 'triggered' sigma. All such extracted time windows were averaged and then plotted. To be clear, the plots in (row 1, column 5) and

(row 5, column 1) were generated from the same underlying dataset, namely time traces from the P_B-cfp, P_D-yfp strain. Each trace is the average of at least 75 peaks, and the shaded error bars are s.e.m..

The 'L-plots' in Figure 5C were made from promoter activity traces, where pulses were identified with MATLAB's findpeaks function, in which the minpeakheight option was set to 3 standard deviations above the mean activity. Each point in the scatter represents a timepoint in which findpeaks identified a peak in either the CFP or YFP promoter activity traces (or both).

Chapter 3 σ^W creates asymmetry in sigma factor competition

3.1 Results

In this project, we ask a very simple question: do *B. subtilis* sigma factors compete for limited supply of core RNAP? Although the literature on competition is extensive, most studies have been conducted in *E.coli*, and there are only a few studies in *B. subtilis*. Moreover, although these studies in *B. subtilis* suggest the existence of competition, they do not strongly rule it in[94].

B. subtilis represents an attractive system to study competition between sigma factors. *B. subtilis* has 12 alternative sigma factors not involved in sporulation, and many are active in the same experimental condition (Figure 3.1A, Figure 2.1A). In this study, we focus on 7 alternative sigmas factors, σ^B, σ^D, σ^L, σ^M, σ^W, σ^X, and σ^Y, which are all active in minimal media plus 40 μg/ml MPA.

We started investigating competition by asking, how does removing one class of sigma factor affect the activity of another sigma factor? For instance, how would removing σ^B from *B. subtilis* affect the remaining sigmas, such as σ^M or σ^X? If sigmas compete for RNAP, then removal of one class of sigma factor would free up more core RNAP for the other classes of sigmas; thus the other sigmas should become more active. However, if sigmas do not compete for RNAP, then removal of one class of sigma factor should have little effect on the others.

To systematically remove individual classes of sigma factors and study their effect on other sigma factors, we constructed a 7x7 ‘deletion’ matrix of strains. Each matrix strain is genetically deleted for one sigma

factor, and also reports on the activity of another sigma factor, where activity is read out via a fluorescent reporter. Sigma deletions represent a perturbation that is of physiological dosage, unlike overexpression experiments that may produce a protein to expression levels well beyond its natural range. We grew these strains in SMM plus 40 μg/ml MPA, an experimental condition shown in Chapter 2 to broadly activate many sigma factors, and then used fluorescence microscopy to quantify sigma-driven fluorescence.

The expected result if competition exists, and if all sigma factors have roughly equivalent properties, is that deletion of one sigma should result in a small increase in another sigma's activity (Figure 3.1.1.B). For instance, we consider 7 classes of sigmas, σ^1 through σ^7, that share a limited amount of core RNAP, whose quantity we designate with R. Then each of σ^1 through σ^7 receive $\frac{R}{7}$ amount of core RNAP. Now if we remove σ^1 from the system, the remaining 6 sigma factors each receive $\frac{R}{6}$ amount of core RNAP, which is ~17% increase over how much core RNAP each sigma factor had originally (Figure 3.1.B)

But the experiments showed us something quite different. Deletion of most sigma factors resulted in strong upregulation of σ^W activity, but had relatively minimal effect on the other sigmas(Figure 3.1C). In addition, deletion of σ^D resulted in most other sigmas becoming upregulated. The effects in the deletion matrix outside of the Δ*sigD* row and the σ^W column are clustered around 1, implying that there is no overall bias when the effects outside the Δ*sigD* row and the σ^W column are considered together (Figure 3.1D) Together, these results suggested a strong asymmetry exists in the system, an effect that would be missed in a less systematic study focusing on only one or two sigma pairs.

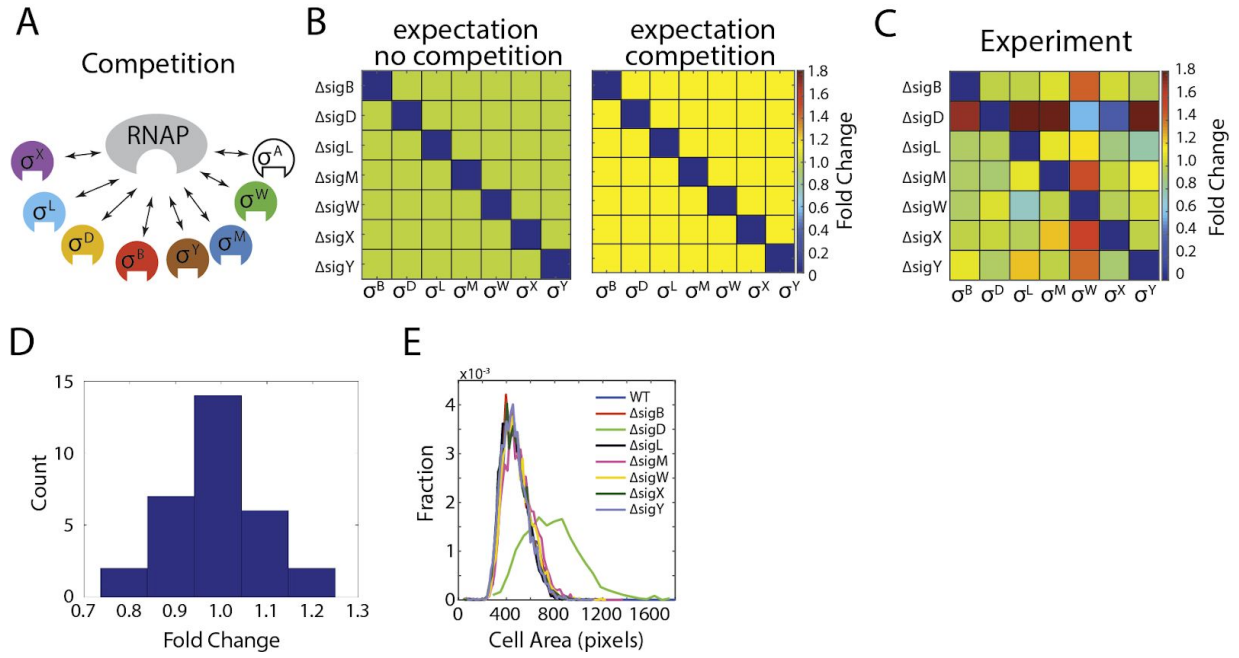

Figure 3.1. σ^W behaves asymmetrically in sigma factor competition. (A) Cartoon of sigma factors competing for core RNAP. (B) Schematic of expected results from deletion matrix. Each colored entry in the grid represents a single deletion matrix strain. The color represents the fold change in sigma factor activity upon deleting another sigma factor. Without competition, we expect non-diagonal matrix entries to be 1, represented by green. With competition, we expect a change of ratio of 1.17 (see main text), represented by yellow. Notice the diagonal elements should be 0, represented by blue. (C) Experimental results from the deletion matrix. (D) Histogram of the ratios shown in panel C, except the ΔsigD row and the σ^W column values have been removed. (E) Histogram of cell areas for the various sigma deletion strains. The outlier histogram is for the ΔsigD strain.

Next, we asked whether sigma deletions have any pleiotropic effects, which would complicate the interpretation of the deletion matrix results. To assess for pleiotropy, we extracted cell size from the microscopy images, and asked whether the sigma deletions had any effect on cell size. We plotted the histogram of cell sizes for each of the sigma factor deletion strains (Figure 3.1.2). We found that deleting sigD significantly increased cell size, but the other sigma deletions did not. Since cell size is associated with increased transcriptional and translational capacity, it is difficult to interpret the ΔsigD row in terms of competition. We therefore do not consider this row in further calculations.

The deletion matrix with a 'column' effect (Figure 3.1.1C) can be explained by 2 possible mechanisms. The first possible mechanism is that most alternative sigma factors drive production of a negative regulator of σ^W. In this scenario, deleting any sigma would reduce the cellular concentration of this putative σ^W negative regulator, thus allowing σ^W to be more active. There could be a single negative σ^W regulator that is driven by many sigma factors, or alternatively, there could many negative σ^W regulators, each driven by one or more different sigma factors. However, there are no known negative regulators of σ^W that would fit into this mechanism (though that does not preclude its existence).

In contrast, we can consider a second mechanism: The observation that deleting most any sigma has the same pattern of effect in the deletion matrix suggests that every sigma is acting through some common mechanism or molecule. The natural candidate for this common molecule is core RNAP, since all sigma factor bind to this molecule. This mechanism is appealing because it does not invoke many putative negative regulators of σ^W, and can potentially explain all of the data with only sigma factors and core RNAP.

To quantitatively explore how competition alone could give rise to the deletion matrix, we constructed a minimal mathematical model of sigma factor competition, in which 7 classes of sigma factors compete to bind core RNAP (Figure 3.2A). The model consisted of 7 chemical reactions, and we solved the concentrations of each component at steady state, using parameters set at physiologically reasonable levels[11,22,95]. Importantly, all sigma factors were symmetric with respect to one another, meaning the deletion matrix from this model must be symmetric.

We then asked in the model whether we could reproduce a deletion matrix with a strong 'column' effect, specifically by adjusting the affinity and abundance of only one sigma factor. We undertook a parameter

search in the model, varying one sigma factor's affinity and abundance, and asking how these variations affected the deletion matrix (Figure 3.2B). And we found one region in parameter space that could reproduce the deletion matrix (Figure 3.2B,C).

This region in parameter space was to take one sigma factor, and reduce its affinity by a factor of 10 and increase its abundance by a factor 3. These changes are well within reported differences in sigma factor affinities[95]. This 'weaker' sigma is weaker at competing against the other 'generic' sigmas, so it is generally less able to bind to core RNAP, and leads to the 'column' effect in the deletion matrix.

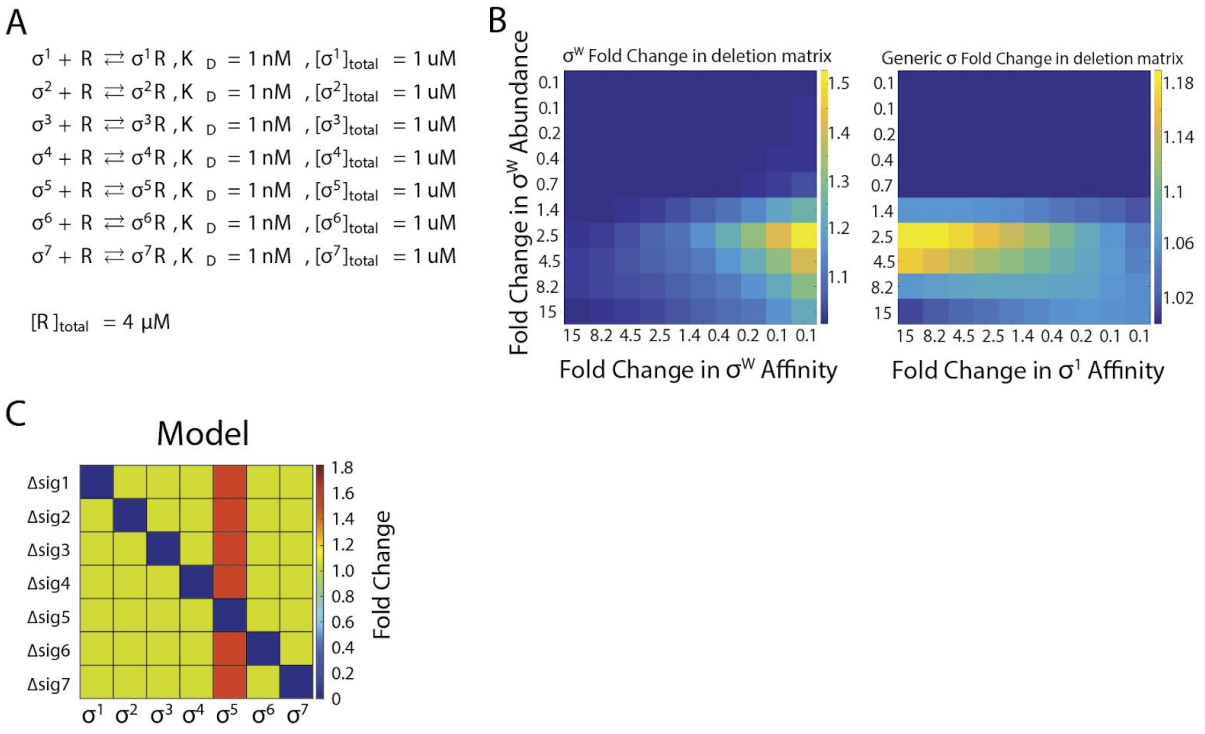

Figure 3.2. Model of asymmetric sigma factor competition. (A) The toy model considers 7 reactions, for 7 sigma factors interacting with a limited supply of core RNAP. (B) Parameter search results. The model started with all sigmas symmetric, with the parameters listed in panel A. The parameter search was done by varying the parameters for only 1 sigma factor, called σ^W. More specifically, the parameter search was on a grid, where one axis is σ^W affinity for core RNAP, and the other axis is σ^W abundance. Notice in the left matrix that low σ^W affinity leads to the desired effect, where deletion of any sigma leads to high fold change in σ^W activity (with the obvious exception that deleting σ^W leads to a fold change of 0 for σ^W activity). Similarly, the right matrix shows that at low affinity and high abundance for σ^W, deleting any sigma leads to relatively lower fold change in a non-

σ^W sigma. (C) The deletion matrix from the toy model, using the parameter values identified from panel B. All sigmas are symmetric in the model except for σ^5, which has lower affinity and higher abundance compared to the other sigmas.

Although the model faithfully reproduced the main features of deletion matrix, we tested it further by using it to make predictions. In particular, the model predicts that overexpression of a generic sigma has different effects on the weak sigma versus another generic sigma (Figure 3.3A). According to the model, overexpressing a generic sigma has little effect on another generic sigma, but strongly represses the weak sigma. We then tested the veracity of these predictions experimentally. We overexpressed σ^B, one of the generic sigma factors, and measured the effect on σ^W, the weak sigma, and on σ^D, σ^M, and σ^X, generic sigmas (Figure 3.3B,C). And we found that the experiments matched the model's predictions. Overexpression of σ^B inhibited σ^W activity but not the other sigmas. We emphasize that the model's parameters were set to match the deletion matrix data, and not to these overexpression experiments. And together, these experiments represent a partial 'row' of an overexpression matrix. In the overexpression matrix, every strain overexpresses one sigma factor and reports on another sigma.

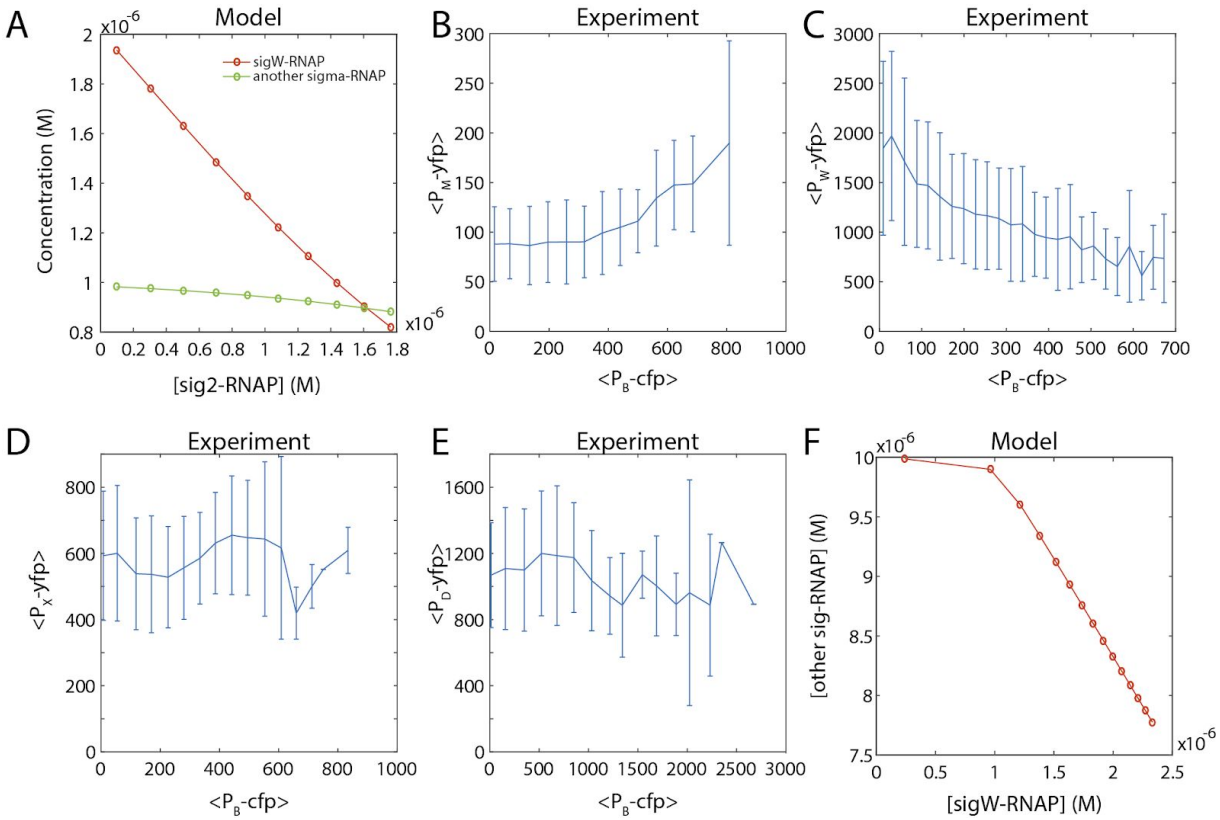

Figure 3.3. Predictions from the toy model match experiments. (A) Prediction from the toy model for sigma overexpression experiments. Overexpression of a 'generic' sigma factor strongly decreases σ^W, the weak sigma,as seen in the red curve). However, the same perturbation has minimal effects on another generic sigma. (B) Effect of σ^B overexpression on σ^W and σ^D activity. Notice σ^B, a generic sigma, inhibits σ^W but not σ^D, consistent with the prediction in panel A. (C) Effect of σ^B overexpression on σ^M and σ^X activity, in the left and right plots, respectively. The left plot, for instance, contains two histograms, and each histogram is the single cell distribution of σ^M driven fluorescence. The two histograms differ in that they compare zero vs max σ^B induction. Notice that σB induction has little effect on σ^M and σ^X (D). Prediction from the toy model for the effect of σ^W overexpression on other sigmas. This prediction has not been confirmed experimentally.

3.2 Discussion and Future Directions

Together, our results suggest that core RNAP is limiting in *B. subtilis*. We systematically explored all pairwise functional relationships between 7 alternative sigma factors using our deletion matrix. The deletion matrix revealed that deleting most any sigma factor preferentially increases the activity of one sigma factor, σ^W. We then demonstrated with a simple mathematical model that these results are consistent with competition for core RNAP, where one sigma factor has relatively low affinity but high

abundance. We further tested the model's predictions by investigating a row of the overexpression matrix, and showed that the model's prediction are matched by experiment.

We note that all of these results could in theory be the result of specific regulation between σ^W and the rest of the sigmas, and that we do not rule out this possibility per se. However, we would argue that our interpretation explains the experimental results in terms of known parameters and interactions, whereas the specific regulation hypothesis requires invoking multiple, putative regulatory connections.

We also report the surprising finding that sigma factor competition is highly asymmetric, where σ^W is a 'weak' factor in a sea of 'generic' sigma factors. This can create an odd situation where 2 sigmas seemingly do not compete with one another, even when core RNAP is limited. That is, overexpression of a generic sigma depletes σ^W from core RNAP before affecting any other sigma (Figure 3.3A,B,C). Indeed, a study that focuses on competition between generic sigma factors could mistakenly conclude that competition for core RNAP does not even exist. In this way, the fraction of core RNAP bound by σ^W represents a 'free pool' that is easily accessible to the other sigma factors. Why the cell would have σ^W stand apart in this way is an open question.

That the toy model can reproduce the main experimental features of the model is surprising, since it effectively ignores many layers of sigma factor regulation. Many sigma factors are positively and negatively regulated, and each sigma factor typically has idiosyncratic regulation. However, the system behaves in a fashion where average sigma competition can be simply explained by effective abundances and affinities, without need to include the various feedback loops and regulatory arrows. Although these kinds of regulations are surely important at the single cell level[68], here we propose that they may not have a strong effect on average sigma behavior.

In future work, we propose to systematically explore the rest of the overexpression matrix. Although we have experimentally tested one 'row' of an overexpression matrix (Figure 3.3), it would be informative to measure the other rows. In particular, we expect the overexpression matrix to have a 'column' effect, where overexpression of most any sigma strongly inhibits σ^W but not the other sigmas. One interesting row to investigate is be the σ^W overexpression row. The model predicts an interesting effect of σ^W overexpression, where σ^W has little effect on the other sigmas until its levels reach some threshold, and then transitions to sharply inhibiting the other sigmas (Figure 3.3D).

Future work would also include measurements of sigma factor binding affinities and abundances, specifically to examine whether σ^W indeed has lower binding affinity core RNAP, and whether it is more relatively more abundant. However, the interpretation on σ^W abundance may be difficult. Due to the presence of anti-sigmas and anti-anti sigmas, it is hard to estimate from abundances alone how much σ^W is actually actively competing for core RNAP.

Additional modeling work could include 1) modeling the effect of σ^A, the housekeeping sigma factor, and 2) systematically varying the amount of total RNAP to ensure these results are not dependent on the specific choice of total RNAP, and 3) relating these modeling results back to the full model described in Chapter 2.

It is quite possible, however, that the affinity of σ^W for core RNAP is not appreciably lower than those of the other sigmas, and that the underlying mechanism is something different entirely. In this case, we will examine other differences between sigma factors as the source of the asymmetric competition. In particular, we plan to consider the the feedback loops and additional interactions that we so blithely

brushed away a few paragraphs ago. For instance, in the full model of sigma factor activity shown in Chapter 2, it is possible to recreate the column effect of the deletion matrix by reducing the positive feedback strength of σ^W (result not shown here). Thus we emphasize that there are multiple possible mechanisms that could underlie asymmetric competition, and we leave it to future studies to elucidate which are the most significant.

3.3. Materials and Methods

All experimental methods were as in Chapter 2.

3.3.1 Modeling

The modeling considered 8 chemical species, RNAP and 7 classes of sigma factors, the latter denoted σ_1 through σ_7. Each sigma factor could bind to RNAP, where the binding equilibrium was governed by dissociation constants K_1 through K_7, for σ_1 through σ_7 respectively. The abundance of each sigma factor was initially set at 1 μM, the abundance of RNAP at 4 μM, and all dissociation constants at 1 nM, which are physiologically reasonable[48]. Thus the system was governed by 7 chemical equations shown below:

$$\sigma_1 + R \rightleftarrows \sigma_1 R \ , K_D = 1\,\mathrm{nM} \ , [\sigma_1]_{total} = 1\,\mathrm{uM}$$
$$\sigma_2 + R \rightleftarrows \sigma_2 R \ , K_D = 1\,\mathrm{nM} \ , [\sigma_2]_{total} = 1\,\mathrm{uM}$$
$$\sigma_3 + R \rightleftarrows \sigma_3 R \ , K_D = 1\,\mathrm{nM} \ , [\sigma_3]_{total} = 1\,\mathrm{uM}$$
$$\sigma_4 + R \rightleftarrows \sigma_4 R \ , K_D = 1\,\mathrm{nM} \ , [\sigma_4]_{total} = 1\,\mathrm{uM}$$
$$\sigma_5 + R \rightleftarrows \sigma_5 R \ , K_D = 1\,\mathrm{nM} \ , [\sigma_5]_{total} = 1\,\mathrm{uM}$$
$$\sigma_6 + R \rightleftarrows \sigma_6 R \ , K_D = 1\,\mathrm{nM} \ , [\sigma_6]_{total} = 1\,\mathrm{uM}$$
$$\sigma_7 + R \rightleftarrows \sigma_7 R \ , K_D = 1\,\mathrm{nM} \ , [\sigma_7]_{total} = 1\,\mathrm{uM}$$

$$[R]_{total} = 4\,\mu M$$

Chemical Equations and Initial Parameter Set. All dissociations constants were set at 1nM, all total sigma abundances at 1 μM, and the total RNAP abundance at 4 μM.

Analysis of the system above, as well as all other analyses, was done at steady state. To solve for the steady state of the system, each equation above was first re-arranged to be expressed in terms of the RNAP-σ complexes. For instance, the equation for σ_1 was re-arranged as below:

$$\frac{\sigma_1 R}{\sigma_1 \times R} = K_{D1}$$

$$\frac{\sigma_1 R}{(\sigma_{1tot} - \sigma_1 R) \times R} = K_{D1}$$

$$\frac{\sigma_1 R}{(\sigma_{1tot} - \sigma_1 R) \times (R_{tot} - \sum_{k=1}^{7} \sigma_k R)} = K_{D1}$$

Rearrangement of the equilibrium binding equation for σ_1. The term σ_1, which represents the concentration of free σ_1, has been replaced by a term representing the difference between the total σ_1 concentration and the complex σ_1R. Similarly, the term R, which represents the concentration of free RNAP, has been replaced with a term representing the difference between the total RNAP concentration and the sum of all concentrations of σ_1R through σ_7R.

The same rearrangement shown above for σ_1 was then done for all 7 sigma factors, leading to the below system of 7 equations:

$$\frac{\sigma_1 R}{(\sigma_{1tot} - \sigma_1 R) \times (R_{tot} - \sum_{k=1}^{7} \sigma_k R)} = K_{D1}$$

$$\frac{\sigma_2 R}{(\sigma_{1tot} - \sigma_2 R) \times (R_{tot} - \sum_{k=1}^{7} \sigma_k R)} = K_{D2}$$

$$\frac{\sigma_3 R}{(\sigma_{1tot} - \sigma_3 R) \times (R_{tot} - \sum_{k=1}^{7} \sigma_k R)} = K_{D3}$$

$$\frac{\sigma_4 R}{(\sigma_{1tot} - \sigma_4 R) \times (R_{tot} - \sum_{k=1}^{7} \sigma_k R)} = K_{D4}$$

$$\frac{\sigma_5 R}{(\sigma_{1tot} - \sigma_5 R) \times (R_{tot} - \sum_{k=1}^{7} \sigma_k R)} = K_{D5}$$

$$\frac{\sigma_6 R}{(\sigma_{1tot} - \sigma_6 R) \times (R_{tot} - \sum_{k=1}^{7} \sigma_k R)} = K_{D6}$$

$$\frac{\sigma_7 R}{(\sigma_{1tot} - \sigma_7 R) \times (R_{tot} - \sum_{k=1}^{7} \sigma_k R)} = K_{D7}$$

System of 7 equations. Each equation is simply the re-arrangement of the chemical equilibrium equation of a sigma factor binding to RNAP, and there are 7 total equations for 7 sigma factors.

The above system of 7 equations has exactly 7 unknowns, namely σ_1R…σ_7R. All other terms are either equilibrium constants, the *total* concentration of a sigma factor, or the total concentration of RNAP, all of which are predetermined values. The solution of this system is the steady state values of σ_1R…σ_7R. To find this solution, we used the vpasolve command in MATLAB 2016a. Any results from vpasolve that contained negative or complex solutions was discarded.

For any sigma factor, the two 'knobs' that can affects its behavior are its total abundance and its K_D. These two knobs were systematically varied to search for a parameter regime that replicated the effects of the experimental knockout matrix. Finally, yo model the deletion of any sigma factor, the system of equations was simply solved for remaining 6 sigma factors rather than 7.

Chapter 4. Cell death activates σ^X in neighboring cells, a novel mode of sigma activation

4.1 Introduction

Alternative sigma factors respond to a wide variety of stresses. For instance, the general stress response factor σ^B of *B. subtilis* activates when cells enter stressful stationary phase[28]. σ^B also activates in response to heat and ethanol stress[96]. Similarly, σ^L protects against cold stress[33], whereas σ^Y responds to nitrogen deprivation[97]. Sigma factors also respond to a wide variety of small molecules or proteins: σ^V protects against lysozyme[98], and σ^W and σ^M against cell wall antibiotics induce σ^W and σ^M [99].

Here we report a novel activator of sigma factors. We show that cell lysis causes adjacent cells to activate σ^X, which is a previously unreported activator for σ^X and more broadly for sigma factors. We observe this effect in multiple experimental conditions. In addition, isolated cell extract activates σ^X, suggesting that cell lysis contains some chemical or agent that is a σ^X activator. This effect is specific to σ^X, as cell lysis only has minimal effects on other sigmas.

Unlike Chapter 2, this chapter is unpublished work. I end the chapter with discussion on the future directions for this project. In particular, I propose that cell death and σ^X act in concert to form wrinkles in biofilms.

4.2 Results

This project was borne out of a screen, where we were testing different chemical compounds for their effects on sigma factors. One of the compounds we tested was the antibiotic bacitracin, which was previously reported to activate σ^X in batch culture experiments[70]. Since previous studies have shown that

sigma factors activate heterogeneously at the single cell level (see Chapter 2), we asked whether bacitracin could have interesting effects on σ^X when studied in single cells. To examine the single cell activity of σ^X, we obtained timelapse microscopy of growing microcolonies of the P_X-yfp reporter strain, grown on agarose pads supplemented with Spizizen's Minimal Medium (SMM-Agarose pads) and 30 μg/ml bacitracin.

And we observed something unexpected. We found that cell lysis precedes activation of σ^X in cells neighboring that lysed cell (Figure 4.1A). Within 15 min of a cell lysis event, we saw clear activation of σ^X in neighboring cells. We next asked how long σ^X is active following a cell lysis event. To do so, we calculated the derivative of the yfp fluorescent signal, since the yfp protein is stable. We call this derivative the 'promoter activity'. These calculations revealed that the σ^X activity post-lysis lasts for roughly 90 min (Figure 4.1B). We believe this timescale is set by the cell lysis contents being diluted out into the rest of the agarose pad. In addition, every cell lysis event we observed led to increased σ^X activity in neighboring cells. Conversely, we also found that for every cluster of cells simultaneously active in σ^X, there was at least 1 cell lysis event preceding it within 45 min. However, σ^X activity was not strictly dependent on cell lysis (Figure 4.1A), as we observed cells active in σ^X that had not been previously exposed to a cell lysis event.

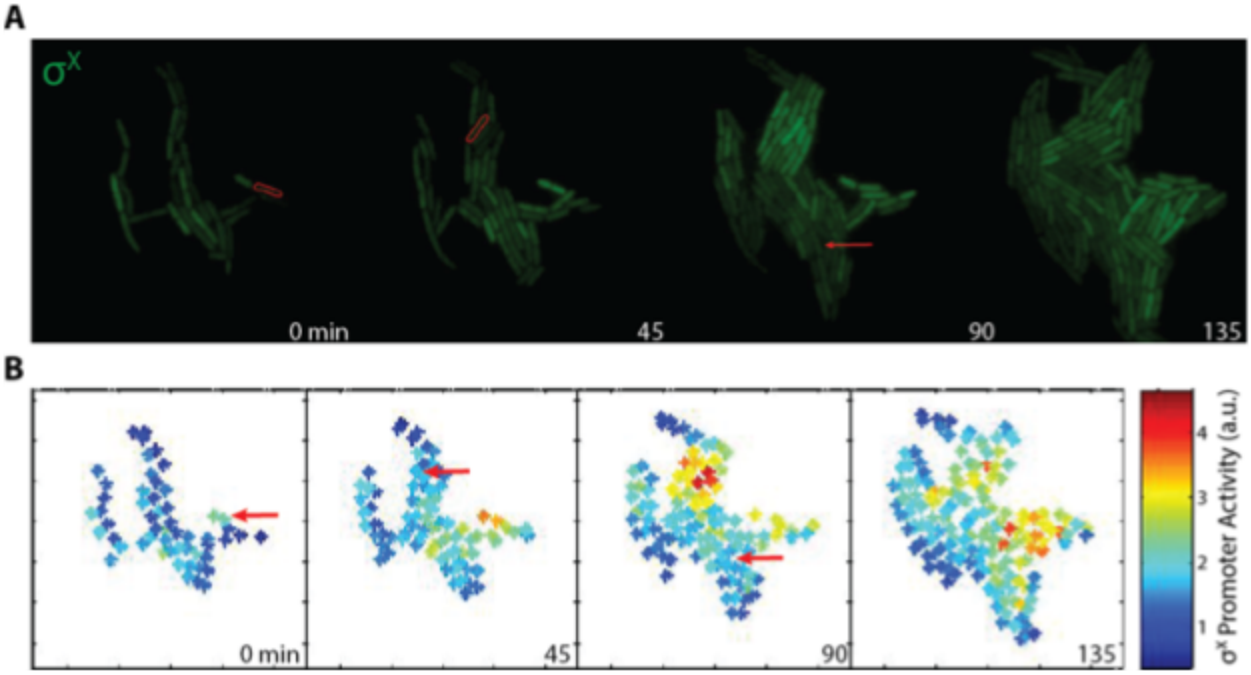

Figure 4.1. Cell death precedes activation of σ^X in neighboring cells. (A) Filmstrip of a growing microcolony of *B. subtilis*, where the cells carry a P_X-yfp reporter. Microcolonies were grown on SMM-Agarose pads supplemented with 30 μg/ml bacitracin. Cells outlined in red will lyse within the next 15 minutes. The red arrow in t = 90 min panel indicates the location of a cell that had lysed within the past 15 minutes. (B) Schematic representation of the growing microcolony. The location of each asterisk represents the centroid of a single cell, and the color of the asterisk corresponds to that cell's σ^X promoter activity. Red arrows indicates cells that are about to lyse, or have recently lysed. Notice that cell surrounding a lysed cell increased their σ^X activity by the next panel frame.

We then wondered whether this cell death and σ^X effect is dependent on bacitracin at all. To answer this question, we obtained timelapse movies of the P_X-yfp reporter strain, except this time we did not add any bacitracin. Cells were grown on SMM-agarose pads with no otherwise stress added. And we found that cell death precedes σ^X even without any otherwise stress (Figure 4.2). These results suggest that the link between cell death and σ^X is a general phenomenon not dependent on any particular experimental condition.

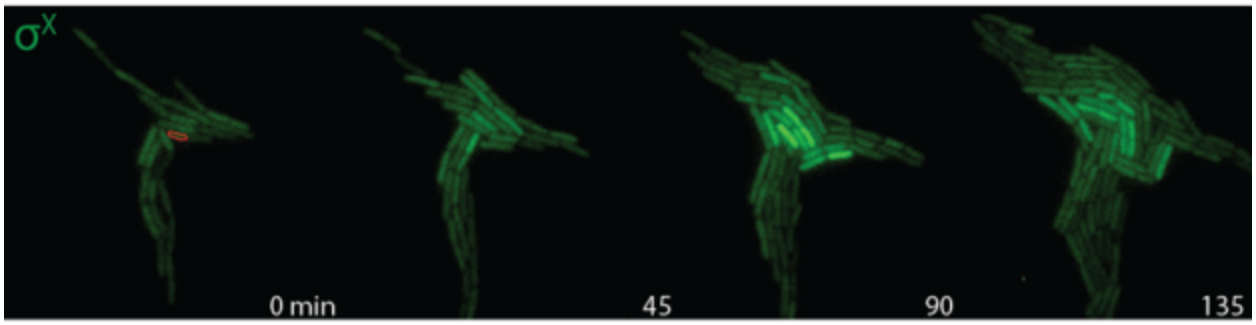

Figure 4.2. Cell death activates σ^X independently of any drug presence. Filmstrip of a growing microcolony of *B. subtilis*, where the cells carry an chromosomally integrated P_X-yfp reporter. Microcolonies were grown on SMM-Agarose pads, importantly not supplemented with any other activators for σ^X . The red-outlined cell will lyse within the next 15 minutes. Notice the activation of σ^X at t = 45 to t=135 min following the lysis of the cell in leftmost panel.

We have so far demonstrated that cell lysis events precede σ^X activity in neighboring cells, but this temporal correlation does not imply causation. To explore this potential causal link between cell death and σ^X , we turned to a cell lysis experiment. We reasoned that if cell lysis causes σ^X to activate in nearby cells, then we should be able to recreate this effect by harvesting our own cell lysate and then adding it to our P_X-yfp reporter. We grew liquid, batch cultures of wildtype *B. subtilis* cells and then harvested the cell lysate with sonication. We added this harvested cell lysate in various amounts to our P_X-yfp reporter, and found that cell lysate activates σ^X dose-dependently (Figure 4.3). In addition, we observed minimal effects on other sigma factors (Figure 4.3). This cell lysate experiment on σ^X was repeated multiple times, but the effect on the sigmas besides σ^X was only repeated once. So it remains to be determined whether the small effects on the other sigmas in Figure 4.3 are reproducible.

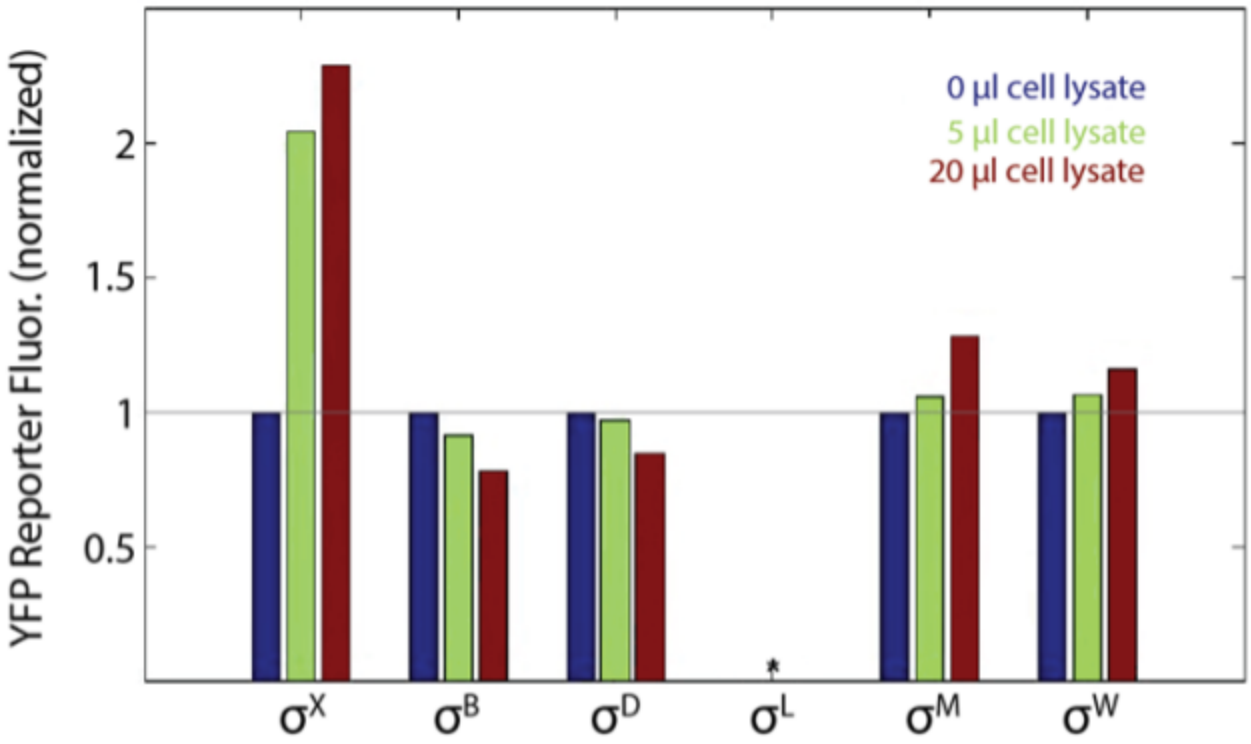

Figure 4.3. Cell lysate strongly activates σ^X relative to other sigma factors. Cell lysate of *B. subtilis* was added to liquid cultures of *B. subtilis* sigma factor reporter strains. σ^X responded dose-dependently to lysate, whereas other sigmas were less affected. Each set of 3 bars for each sigma was normalized to the 0 cell lysate condition. The asterisk for σ^L represents activity indistinguishable from autofluorescence. Note the lack of error bars is due to this experiment being repeated once.

4.3 Future Directions

One possible future direction is to identify the agent in the cell lysis extract that is activating σ^X. The categories of possible agents include nucleic acids, proteins, sugars, cell wall fragments and even lytic viruses. A virus is an attractive possibility, since the observation of cell lysis begs the question, what causes the cell to lyse in the first place? One possibility is a virus, and that σ^X is protecting against the released lytic viruses. However, it is also possible that bacterial cells 'age', and that the old pole cells are the ones that are more likely to lyse than their younger counterparts. It has previously been reported that σ^X protects cationic antimicrobial peptides, and also against H_2O_2[34]. But the agent in the cell extract

A second possible direction is to explore the functional roles could exist for this link between cell death and σ^X. And we found in the literature an interesting possible function in the context of biofilm wrinkle formation. *B. subtilis* colonies when grown in the right conditions exhibit interesting 3D-structures known as *wrinkles* (Figure 4.4A), and it is an open question how these these tortuous wrinkle formations are formed.

One recent study demonstrated that localized, massive cell death precedes wrinkle formation[100] (Figure 4.4B). In addition , they showed induction of cell death in a particular spot in the biofilm induced wrinkles at that spot. Separately, another group showed that genetically deleting *sigX* causes loss of wrinkle formation[101] (Figure 4.4.C).

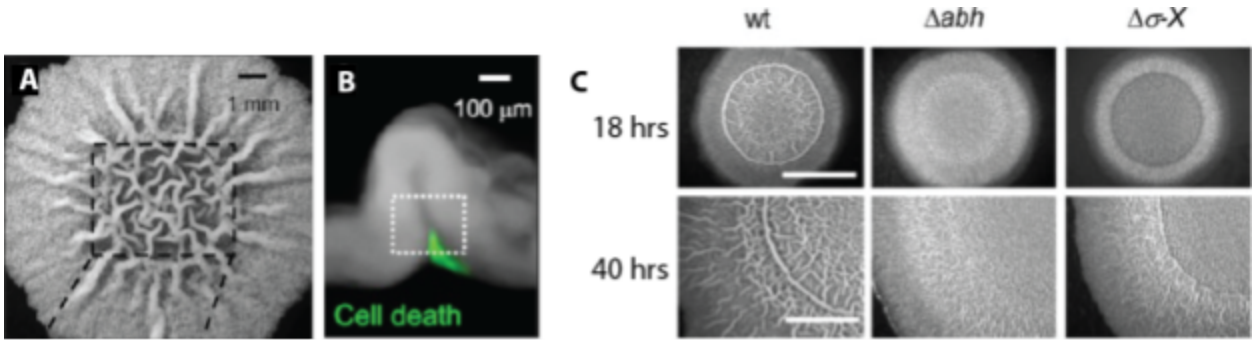

Figure 4.4. There exists a potential role for σ^X and cell death in biofilm wrinkle formation. Both figure panels were modified from previous work and are referenced. (A) Three-day old *B. subtilis* biofilm. Note the wrinkles inside the dotted box. (B) Cell death precedes formation of biofilm wrinkles. Cross-section of a 30 hour old biofilm wrinkle. The green is a Sytox cell death reporter, whereas the gray represents fluorescence from a P_{ftsAZ}-cfp reporter. This panel does not demonstrate that cell death precedes wrinkle formation, it is merely supposed to provide a visual sense of what a wrinkle is and where the cell death would occur. (B) σ^X and its target gene *abh* are required for biofilm wrinkle formation. Three strains were grown under biofilm formation conditions, and imaged at 18 hrs and 40 hrs. The wildtype (wt) strain is the one known under the code number NCIB3610, while the other 2 strains were deleted for *sigX* and *abh* respectively in this same wildtype background. Scale bar is 5mm.

We propose that σ^X provides the missing link between cell death and and wrinkle formation. We hypothesize that a localized area of massive cell death in the biofilm leads to upregulation of σ^X activity in nearby cells, and that σ^X activity plays an important role in forming the wrinkle structure. In particular, we propose the following studies:

1) *Test in the context of biofilms whether cell death causes σ^X to activate in neighboring cells*. These experiments would mimic the experiments described in this chapter, except done in the context of biofilms. It is important to confirm that the link between cell death and σ^X activation exists in biofilms. For instance, the cell lysate in small microcolonies may contain chemical compounds not present in the cell lysate from biofilm cells. In addition, there is a subtle technical reason why the link may not exist in biofilms. The experiments described in this chapter used the *B. subtilis* strain PY79, but studies with biofilms use *B. subtilis* strain 3610[100]. This is chiefly because strain 3610 has the ability to form biofilms while PY79 does not. And different *B. subtilis* strains can exhibit different sigma factor responses to the same stress[29], raising the possibility that PY79 exhibits the link between cell death and σ^X, but strain 3610 does not.

2) *Explore the link between cell death and σ^X in wrinkle formation:* Here we propose experiments to elucidate how these cell death and σ^X interact to drive wrinkle formation.

One possible role for σ^X is that it controls rate of cell death in biofilms. In this scenario, deleting *sigX* leads to decreased cell death, which in turn leads to loss of wrinkles. To test this possibility, we will compare the rates and spatial patterns of cell death in wildtype vs *sigX* deleted biofilms.

A second possible role for σ^X is that activates genes important for wrinkle formation in cells around the site of cell death. To test this possibility, we will perform wrinkle induction experiments in biofilms with the *sigX* deletion background. Induction of wrinkle formation has previously been reported, where inducing cell death in biofilms leads to wrinkle formation at the site of induced cell death[100]. We will induce localized cell death in *sigX* deleted biofilms, and observe whether wrinkles from at the site of cell death. The lack of wrinkle formation would implicate σ^X as necessary in post-cell death context. Finally,

we would propose a rescue experiment, where we induce both cell death and ectopic σ^X in cells surrounding the induced cell death site. However, this experiment may be technically challenging.

A third possible role for σ^X is in wrinkle maintenance. In this scenario, the wrinkles may form normally without σ^X, but become smoothed without σ^X to maintain them. This seems unlikely because if true it would have been noticed by other groups, but we mention it for completeness.

4.4 Materials and Methods

Refer to Chapter 3, both strains and methods are identical to the ones used in that chapter.

Chapter 5 Conclusion

5.1 Summary

In this thesis, I described two projects studying how sigma factors interact with each other, and one project on a novel activation mode and potential function for σ^X.

The first project proposed a novel mode of sharing limited enzymatic machinery that we call timesharing. We showed the alternative sigma factors of *B. subtilis* activate in pulses, compete with another, and have a complex mix of positive and negative correlations. We demonstrated with a mathematical model that mixed correlations are actually consistent with competition, a counterintuitive result that may be relevant to other studies.

The second project showed that competition between sigma factors is highly asymmetric, where σ^W is the weakest sigma. We suggest with a mathematical model that the underlying mechanism is reduced affinity of σ^W for core RNAP, paired with increased abundance of σ^W. The model was fitted to the deletion matrix data, and its prediction for a subset of overexpression experiments was matched by the data. However, we emphasize there are other mechanisms consistent with competition that could also generate the deletion matrix.

The third project demonstrated that cell death activates σ^X in nearby cells. This effect was general across many experimental conditions, and also specific to σ^X. These results suggest that σ^X could be the missing link between cell death and biofilm wrinkle formation.

5.2 Future Work

Here I leave questions to be addressed by future studies

For Chapter 2:

- *How do pulsing, the mixed positive and negative correlations, and the deletion matrix integrate together?* This work is actually ongoing, in the full model of sigma factor pulsing from Chapter 2, we have identified a parameter regime that reproduces all 3 observations of pulsing, mixed correlations, and the striking column effect in the deletion matrix.
- *What is the functional role of pulses?* It has not been shown that sigma factor pulses perform any function. One can imagine adding stress to a population of cells, and observing that cells in the middle of a sigma pulse survive cells not pulsing.
- *How can timesharing be leveraged for synthetic biology?* Timesharing can be used to create a heterogeneous population of cells from the same underlying genome, thus avoiding problems in mixed populations of bacteria where a subpopulation will drop out. This is a project in search of the right context. I toyed with the idea of using two negatively correlated sigma factors to drive two different metabolic programs of glucose and xylose metabolism, as these two metabolic programs are typically at the same time in a single cell.
- *Is pulse generation truly stochastic?* The mother machine data for the first time tracks sigma factor activity over long timescales, enabling analysis of the interpulse time durations.
- *Do two component response regulators exhibit interesting single cell dynamics?* Although activity the two component response regulators have been studied in population averages, their single cell responses remain unclear.
- *More generally, how do we efficiently identify interesting single cell dynamics for future study?* The current method of finding a project is slow. One adds a few different stress to a few different fluorescent reporters and looks for interesting dynamics or heterogeneity. This inefficient search makes it difficult to identify

new areas for studies of single cell dynamics. A multiplexed screen with a library of reporters paired with a library of stress compounds may be one approach.

For Chapter 3:

- *What is the overexpression matrix of sigma factor competition?* The overexpression matrix would complement the deletion matrix. More detailed predictions are discussed in Chapter 3.
- *What are the relative binding affinities and abundances of sigma factors?* These measurements would support or rule out the toy model in Chapter 3.
- *Why would cells want to have σ^W be an effectively weak sigma?* That σ^W is relatively weak may suggest it is the least important for survival. A study of growth rates of the sigma factor deletion strains in a wide variety of stresses may help answer this question.

For Chapter 4:

- *What is in cell lysate that activates σ^X?* One can imagine a fractionation approach that narrows down the identity of the causative agent in cell lysate.
- *How do cell death and σ^X interact to form wrinkles?* This was discussed in detail in Chapter 4.
- *Do lysates from other bacterial organisms activate σ^X?* Alternatively, lysates from other organisms may activate different sigma factors.
- How is σX changing cells' behavior to make them more likely to form wrinkles?

References

1. Chamberlin, M. & Berg, P. DEOXYRIBONUCLEIC ACID-DIRECTED SYNTHESIS OF RIBONUCLEIC ACID BY AN ENZYME FROM ESCHERICHIA COLI. *Proceedings of the National Academy of Sciences* **48,** 81–94 (1962).
2. Burgess, R. R., Travers, A. A., Dunn, J. J. & Bautz, E. K. Factor stimulating transcription by RNA polymerase. *Nature* **221,** 43–46 (1969).
3. Haldenwang, W. G. & Losick, R. A modified RNA polymerase transcribes a cloned gene under sporulation control in Bacillus subtilis. *Nature* **282,** 256–260 (1979).
4. Haldenwang, W. G. & Losick, R. Novel RNA polymerase sigma factor from Bacillus subtilis. *Proceedings of the National Academy of Sciences* **77,** 7000–7004 (1980).
5. Tjian, R. & Losick, R. An immunological assay for the sigma subunit of RNA polymerase in extracts of vegetative and sporulating Bacillus subtilis. *Proc. Natl. Acad. Sci. U. S. A.* **71,** 2872–2876 (1974).
6. Hecker, M., Pané-Farré, J. & Völker, U. SigB-dependent general stress response in Bacillus subtilis and related gram-positive bacteria. *Annu. Rev. Microbiol.* **61,** 215–236 (2007).
7. Ho, T. D., Hastie, J. L., Intile, P. J. & Ellermeier, C. D. The Bacillus subtilis Extracytoplasmic Function σ Factor σ V Is Induced by Lysozyme and Provides Resistance to Lysozyme. *J. Bacteriol.* **193,** 6215–6222 (2011).
8. Guariglia-Oropeza, V. & Helmann, J. D. Bacillus subtilis σ V Confers Lysozyme Resistance by Activation of Two Cell Wall Modification Pathways, Peptidoglycan O-Acetylation and d-Alanylation of Teichoic Acids. *J. Bacteriol.* **193,** 6223–6232 (2011).
9. Devkota, S. R., Kwon, E., Ha, S. C., Chang, H. W. & Kim, D. Y. Structural insights into the regulation of Bacillus subtilis SigW activity by anti-sigma RsiW. *PLoS One* **12,** e0174284 (2017).
10. Schöbel, S., Zellmeier, S., Schumann, W. & Wiegert, T. The Bacillus subtilis sigmaW anti-sigma factor RsiW is degraded by intramembrane proteolysis through YluC. *Mol. Microbiol.* **52,**

1091–1105 (2004).

11. Maaβ, S. *et al.* Highly precise quantification of protein molecules per cell during stress and starvation responses in Bacillus subtilis. *Mol. Cell. Proteomics* **13,** 2260–2276 (2014).
12. Hicks, K. A. & Grossman, A. D. Altering the level and regulation of the major sigma subunit of RNA polymerase affects gene expression and development in Bacillus subtilis. *Mol. Microbiol.* **20,** 201–212 (1996).
13. Farewell, A., Kvint, K. & Nyström, T. Negative regulation by RpoS: a case of sigma factor competition. *Mol. Microbiol.* **29,** 1039–1051 (1998).
14. Jishage, M. & Ishihama, A. Transcriptional Organization and In Vivo Role of theEscherichia coli rsd Gene, Encoding the Regulator of RNA Polymerase Sigma D. *J. Bacteriol.* **181,** 3768–3776 (1999).
15. Jishage, M., Kvint, K., Shingler, V. & Nyström, T. Regulation of ς factor competition by the alarmone ppGpp. *Genes Dev.* **16,** 1260–1270 (2002).
16. Mauri, M. & Klumpp, S. A model for sigma factor competition in bacterial cells. *PLoS Comput. Biol.* **10,** e1003845 (2014).
17. Narula, J., Tiwari, A. & Igoshin, O. A. Role of Autoregulation and Relative Synthesis of Operon Partners in Alternative Sigma Factor Networks. *PLoS Comput. Biol.* **12,** e1005267 (2016).
18. Locke, J. C. W., Young, J. W., Fontes, M., Jimenez, M. J. H. & Elowitz, M. B. Stochastic Pulse Regulation in Bacterial Stress Response. *Science* **334,** 366–369 (2011).
19. Kundu, T. K., Kusano, S. & Ishihama, A. Promoter selectivity of Escherichia coli RNA polymerase sigmaF holoenzyme involved in transcription of flagellar and chemotaxis genes. *J. Bacteriol.* **179,** 4264–4269 (1997).
20. Kusano, S. & Ishihama, A. Stimulatory effect of trehalose on formation and activity of Escherichia coli RNA polymerase E sigma38 holoenzyme. *J. Bacteriol.* **179,** 3649–3654 (1997).
21. Bernardo, L. M. D., Johansson, L. U. M., Solera, D., Skärfstad, E. & Shingler, V. The guanosine

tetraphosphate (ppGpp) alarmone, DksA and promoter affinity for RNA polymerase in regulation of sigma-dependent transcription. *Mol. Microbiol.* **60,** 749–764 (2006).

22. Muntel, J. *et al.* Comprehensive absolute quantification of the cytosolic proteome of Bacillus subtilis by data independent, parallel fragmentation in liquid chromatography/mass spectrometry (LC/MSE). *Mol. Cell. Proteomics* **13,** 1008–1019 (2014).
23. Dufour, A. & Haldenwang, W. G. Interactions between a Bacillus subtilis anti-sigma factor (RsbW) and its antagonist (RsbV). *J. Bacteriol.* **176,** 1813–1820 (1994).
24. Yoshimura, M., Asai, K., Sadaie, Y. & Yoshikawa, H. Interaction of Bacillus subtilis extracytoplasmic function (ECF) sigma factors with the N-terminal regions of their potential anti-sigma factors. *Microbiology* **150,** 591–599 (2004).
25. Siegal-Gaskins, D., Tuza, Z. A., Kim, J., Noireaux, V. & Murray, R. M. Resource usage and gene circuit performance characterization in a cell-free 'breadboard'. *bioRxiv* 000885 (2013).
26. Delumeau, O. *et al.* The dynamic protein partnership of RNA polymerase inBacillus subtilis. *Proteomics* **11,** 2992–3001 (2011).
27. Haldenwang, W. G. The sigma factors of Bacillus subtilis. *Microbiol. Rev.* **59,** 1–30 (1995).
28. Boylan, S. A., Redfield, A. R. & Price, C. W. Transcription factor sigma B of Bacillus subtilis controls a large stationary-phase regulon. *J. Bacteriol.* **175,** 3957–3963 (1993).
29. Wiegeshoff, F., Beckering, C. L., Debarbouille, M. & Marahiel, M. A. Sigma L is important for cold shock adaptation of Bacillus subtilis. *J. Bacteriol.* **188,** 3130–3133 (2006).
30. Helmann, J. D. *et al.* Global transcriptional response of Bacillus subtilis to heat shock. *J. Bacteriol.* **183,** 7318–7328 (2001).
31. Le Jeune, A. *et al.* The extracytoplasmic function sigma factor SigV plays a key role in the original model of lysozyme resistance and virulence of Enterococcus faecalis. *PLoS One* **5,** e9658 (2010).
32. Helmann, J. D. Bacillus subtilis extracytoplasmic function (ECF) sigma factors and defense of the

cell envelope. *Curr. Opin. Microbiol.* **30,** 122–132 (2016).

33. Debarbouille, M., Gardan, R., Arnaud, M. & Rapoport, G. Role of bkdR, a transcriptional activator of the sigL-dependent isoleucine and valine degradation pathway in Bacillus subtilis. *J. Bacteriol.* **181,** 2059–2066 (1999).
34. Cao, M. & Helmann, J. D. The Bacillus subtilis extracytoplasmic-function sigmaX factor regulates modification of the cell envelope and resistance to cationic antimicrobial peptides. *J. Bacteriol.* **186,** 1136–1146 (2004).
35. Helmann, J. D. The extracytoplasmic function (ECF) sigma factors. *Adv. Microb. Physiol.* **46,** 47–110 (2002).
36. Price, C. W. *et al.* Genome-wide analysis of the general stress response in Bacillus subtilis. *Mol. Microbiol.* **41,** 757–774 (2001).
37. Paget, M. S. Bacterial Sigma Factors and Anti-Sigma Factors: Structure, Function and Distribution. *Biomolecules* **5,** 1245–1265 (2015).
38. Gruber, T. M. & Gross, C. A. Multiple Sigma Subunits and the Partitioning of Bacterial Transcription Space. *Annu. Rev. Microbiol.* **57,** 441–466 (2003).
39. Zhang, S. & Haldenwang, W. G. Contributions of ATP, GTP, and redox state to nutritional stress activation of the Bacillus subtilis sigmaB transcription factor. *J. Bacteriol.* **187,** 7554–7560 (2005).
40. Rollenhagen, C. *et al.* Binding of A and B to Core RNA Polymerase after Environmental Stress in Bacillus subtilis. *J. Bacteriol.* **185,** 35–40 (2003).
41. Young, J. W. *et al.* Measuring single-cell gene expression dynamics in bacteria using fluorescence time-lapse microscopy. *Nat. Protoc.* **7,** 80–88 (2011).
42. Dunlop, M. J. Quantitative Single-Cell Gene Expression Measurements in Bacteria Using Time-Lapse Microscopy. *Microsc. Microanal.* **20,** 1174–1175 (2014).
43. Wang, P. *et al.* Robust growth of Escherichia coli. *Curr. Biol.* **20,** 1099–1103 (2010).

44. Taheri-Araghi, S. *et al.* Cell-size control and homeostasis in bacteria. *Curr. Biol.* **25,** 385–391 (2015).

45. Norman, T. M., Lord, N. D., Paulsson, J. & Losick, R. Memory and modularity in cell-fate decision making. *Nature* **503,** 481–486 (2013).

46. Ganguly, A. & Chatterji, D. A comparative kinetic and thermodynamic perspective of the σ-competition model in Escherichia coli. *Biophys. J.* **103,** 1325–1333 (2012).

47. Grigorova, I. L., Phleger, N. J., Mutalik, V. K. & Gross, C. A. Insights into transcriptional regulation and sigma competition from an equilibrium model of RNA polymerase binding to DNA. *Proc. Natl. Acad. Sci. U. S. A.* **103,** 5332–5337 (2006).

48. Maeda, H., Fujita, N. & Ishihama, A. Competition among seven Escherichia coli sigma subunits: relative binding affinities to the core RNA polymerase. *Nucleic Acids Res.* **28,** 3497–3503 (2000).

49. Elowitz, M. B., Levine, A. J., Siggia, E. D. & Swain, P. S. Stochastic gene expression in a single cell. *Science* **297,** 1183–1186 (2002).

50. Volfson, D. *et al.* Origins of extrinsic variability in eukaryotic gene expression. *Nature* **439,** 861–864 (2006).

51. Paulsson, J. Summing up the noise in gene networks. *Nature* **427,** 415–418 (2004).

52. Newman, J. R. S. *et al.* Single-cell proteomic analysis of S. cerevisiae reveals the architecture of biological noise. *Nature* **441,** 840–846 (2006).

53. Bar-Even, A. *et al.* Noise in protein expression scales with natural protein abundance. *Nat. Genet.* **38,** 636–643 (2006).

54. Lin, Y., Sohn, C. H., Dalal, C. K., Cai, L. & Elowitz, M. B. Combinatorial gene regulation by modulation of relative pulse timing. *Nature* **527,** 54–58 (2015).

55. Segrè, D., Deluna, A., Church, G. M. & Kishony, R. Modular epistasis in yeast metabolism. *Nat. Genet.* **37,** 77–83 (2005).

56. Kussell, E. & Leibler, S. Phenotypic diversity, population growth, and information in fluctuating environments. *Science* **309,** 2075–2078 (2005).

57. Thattai, M. & van Oudenaarden, A. Stochastic gene expression in fluctuating environments. *Genetics* **167,** 523–530 (2004).

58. Kussell, E., Kishony, R., Balaban, N. Q. & Leibler, S. Bacterial persistence: a model of survival in changing environments. *Genetics* **169,** 1807–1814 (2005).

59. Veening, J.-W., Smits, W. K. & Kuipers, O. P. Bistability, epigenetics, and bet-hedging in bacteria. *Annu. Rev. Microbiol.* **62,** 193–210 (2008).

60. Kelly, J. L. A New Interpretation of Information Rate. *Bell System Technical Journal* **35,** 917–926 (1956).

61. Beaumont, H. J. E., Gallie, J., Kost, C., Ferguson, G. C. & Rainey, P. B. Experimental evolution of bet hedging. *Nature* **462,** 90–93 (2009).

62. Levine, J. H., Lin, Y. & Elowitz, M. B. Functional roles of pulsing in genetic circuits. *Science* **342,** 1193–1200 (2013).

63. Cai, L., Dalal, C. K. & Elowitz, M. B. Frequency-modulated nuclear localization bursts coordinate gene regulation. *Nature* **455,** 485–490 (2008).

64. Qian, Y., Huang, H.-H., Jiménez, J. & Del Vecchio, D. Resource Competition Shapes the Response of Genetic Circuits. *bioRxiv* 091306 (2017). doi:10.1101/091306

65. Vind, J., Sørensen, M. A., Rasmussen, M. D. & Pedersen, S. Synthesis of Proteins in Escherichia coli is Limited by the Concentration of Free Ribosomes. *J. Mol. Biol.* **231,** 678–688 (1993).

66. Agrawal, G. P. *Fiber-Optic Communication Systems*. (John Wiley & Sons, 2012).

67. Harrison, M. & Wilkes, M. V. Time-Sharing Computer Systems. *Math. Comput.* **24,** 501 (1970).

68. Locke, J. C. W., Young, J. W., Fontes, M., Hernández Jiménez, M. J. & Elowitz, M. B. Stochastic pulse regulation in bacterial stress response. *Science* **334,** 366–369 (2011).

69. Luo, Y. & Helmann, J. D. Extracytoplasmic function sigma factors with overlapping promoter specificity regulate sublancin production in Bacillus subtilis. *J. Bacteriol.* **191,** 4951–4958 (2009).

70. Cao, M. & Helmann, J. D. Regulation of the Bacillus subtilis bcrC bacitracin resistance gene by two extracytoplasmic function sigma factors. *J. Bacteriol.* **184,** 6123–6129 (2002).

71. Steinmetz, M. & Richter, R. Plasmids designed to alter the antibiotic resistance expressed by insertion mutations in Bacillus subtilis, through in vivo recombination. *Gene* **142,** 79–83 (1994).

72. Helmann, J. D., Márquez, L. M. & Chamberlin, M. J. Cloning, sequencing, and disruption of the Bacillus subtilis sigma 28 gene. *J. Bacteriol.* **170,** 1568–1574 (1988).

73. Cao, M. *et al.* Regulation of the Bacillus subtilis Extracytoplasmic Function Protein σY and Its Target Promoters. *J. Bacteriol.* **185,** 4883–4890 (2003).

74. Koo, B.-M. *et al.* Construction and Analysis of Two Genome-Scale Deletion Libraries for Bacillus subtilis. *Cell Syst* (2017). doi:10.1016/j.cels.2016.12.013

75. Eldar, A. *et al.* Partial penetrance facilitates developmental evolution in bacteria. *Nature* **460,** 510–514 (2009).

76. Middleton, R. & Hofmeister, A. New shuttle vectors for ectopic insertion of genes into Bacillus subtilis. *Plasmid* **51,** 238–245 (2004).

77. Kalman, S., Duncan, M. L., Thomas, S. M. & Price, C. W. Similar organization of the sigB and spoIIA operons encoding alternate sigma factors of Bacillus subtilis RNA polymerase. *J. Bacteriol.* **172,** 5575–5585 (1990).

78. Boylan, S. A., Redfield, A. R., Brody, M. S. & Price, C. W. Stress-induced activation of the sigma B transcription factor of Bacillus subtilis. *J. Bacteriol.* **175,** 7931–7937 (1993).

79. Estacio, W., Anna-Arriola, S. S., Adedipe, M. & Márquez-Magaña, L. M. Dual promoters are responsible for transcription initiation of the fla/che operon in Bacillus subtilis. *J. Bacteriol.* **180,** 3548–3555 (1998).

80. Horsburgh, M. J. & Moir, A. Sigma M, an ECF RNA polymerase sigma factor of Bacillus subtilis 168, is essential for growth and survival in high concentrations of salt. *Mol. Microbiol.* **32,** 41–50 (1999).

81. Cao, M., Wang, T., Ye, R. & Helmann, J. D. Antibiotics that inhibit cell wall biosynthesis induce expression of the Bacillus subtilis sigma(W) and sigma(M) regulons. *Mol. Microbiol.* **45,** 1267–1276 (2002).

82. Huang, X., Decatur, A., Sorokin, A. & Helmann, J. D. The Bacillus subtilis sigma(X) protein is an extracytoplasmic function sigma factor contributing to survival at high temperature. *J. Bacteriol.* **179,** 2915–2921 (1997).

83. Spizizen, J. TRANSFORMATION OF BIOCHEMICALLY DEFICIENT STRAINS OF BACILLUS SUBTILIS BY DEOXYRIBONUCLEATE. *Proc. Natl. Acad. Sci. U. S. A.* **44,** 1072–1078 (1958).

84. Young, J. W. *et al.* Measuring single-cell gene expression dynamics in bacteria using fluorescence time-lapse microscopy. *Nat. Protoc.* **7,** 80–88 (2011).

85. Espinar, L., Dies, M., Cagatay, T., Süel, G. M. & Garcia-Ojalvo, J. Circuit-level input integration in bacterial gene regulation. *Proc. Natl. Acad. Sci. U. S. A.* **110,** 7091–7096 (2013).

86. Norman, T. M., Lord, N. D., Paulsson, J. & Losick, R. Memory and modularity in cell-fate decision making. *Nature* **503,** 481–486 (2013).

87. Helmann, J. D. The extracytoplasmic function (ECF) sigma factors. *Adv. Microb. Physiol.* **46,** 47–110 (2002).

88. Li, G.-W., Burkhardt, D., Gross, C. & Weissman, J. S. Quantifying absolute protein synthesis rates reveals principles underlying allocation of cellular resources. *Cell* **157,** 624–635 (2014).

89. Taniguchi, Y. *et al.* Quantifying E. coli proteome and transcriptome with single-molecule sensitivity in single cells. *Science* **329,** 533–538 (2010).

90. Friedman, N., Cai, L. & Xie, X. S. Linking stochastic dynamics to population distribution: an analytical framework of gene expression. *Phys. Rev. Lett.* **97,** 168302 (2006).

91. Raj, A., Peskin, C. S., Tranchina, D., Vargas, D. Y. & Tyagi, S. Stochastic mRNA synthesis in mammalian cells. *PLoS Biol.* **4,** e309 (2006).

92. Rosenfeld, N., Young, J. W., Alon, U., Swain, P. S. & Elowitz, M. B. Gene regulation at the single-cell level. *Science* **307,** 1962–1965 (2005).

93. Lin, Y., Sohn, C. H., Dalal, C. K., Cai, L. & Elowitz, M. B. Combinatorial gene regulation by modulation of relative pulse timing. *Nature* **527,** 54–58 (2015).

94. Hicks, K. A. & Grossman, A. D. Altering the level and regulation of the major sigma subunit of RNA polymerase affects gene expression and development in Bacillus subtilis. *Mol. Microbiol.* **20,** 201–212 (1996).

95. Maeda, H., Fujita, N. & Ishihama, A. Competition among seven Escherichia coli sigma subunits: relative binding affinities to the core RNA polymerase. *Nucleic Acids Res.* **28,** 3497–3503 (2000).

96. Ferreira, A., O'Byrne, C. P. & Boor, K. J. Role of sigma(B) in heat, ethanol, acid, and oxidative stress resistance and during carbon starvation in Listeria monocytogenes. *Appl. Environ. Microbiol.* **67,** 4454–4457 (2001).

97. Tojo, S. *et al.* Organization and expression of the Bacillus subtilis sigY operon. *J. Biochem.* **134,** 935–946 (2003).

98. Guariglia-Oropeza, V. & Helmann, J. D. Bacillus subtilis σ(V) confers lysozyme resistance by activation of two cell wall modification pathways, peptidoglycan O-acetylation and D-alanylation of teichoic acids. *J. Bacteriol.* **193,** 6223–6232 (2011).

99. Helmann, J. D. Bacillus subtilis extracytoplasmic function (ECF) sigma factors and defense of the cell envelope. *Curr. Opin. Microbiol.* **30,** 122–132 (2016).

100. Asally, M. *et al.* Localized cell death focuses mechanical forces during 3D patterning in a biofilm.

Proc. Natl. Acad. Sci. U. S. A. **109,** 18891–18896 (2012).

101. Murray, E. J., Strauch, M. A. & Stanley-Wall, N. R. SigmaX is involved in controlling Bacillus subtilis biofilm architecture through the AbrB homologue Abh. *J. Bacteriol.* **191,** 6822–6832 (2009).